https://doi.org/10.5194/egusphere-2024-2034
Preprint. Discussion started: 15 July 2024

Insights into the tectonic evolution of the Svecofennian orogeny based on *in situ* Lu-Hf dating of garnet from Olkiluoto, SW Finland

JON ENGSTRÖM [1,2*], KATHRYN CUTTS[1], STIJN GLORIE[3] ESA HEILIMO[4] ESTER M. JOLIS[1] AND RADOSLAW M. MICHALLIK[1]

[1]*Geological Survey of Finland, P.O. Box 96, FI-02151 Espoo Finland.*

[2]*Åbo Akademi University, Akatemiakatu 1, 20500 Turku*

[3]*Department of Earth Sciences, University of Adelaide, Adelaide, SA 5005, Australia*

[4]*University of Turku, Akatemiakatu 1, 20500 Turku*

* Corresponding author (e-mail: jon.engstrom@gtk.fi)

Abstract. The Southern Finland granites and associated migmatitic rocks have a complex metamorphic history, being affected by multiple events during the ca. 1.88-1.79 Ga Svecofennian orogeny. In this study, the prolonged tectonic evolution of migmatites and associated rocks in SW Finland has been studied using the new *in situ* Lu-Hf method. Results reveal detailed temporal constraints for the tectonic evolution that can be linked to major events in adjacent tectonic blocks in both Finland and Sweden during the Svecofennian orogeny. The metamorphic peak at the Olkiluoto site occurred at 1834 ± 7 Ma based on *in situ* Lu-Hf dating of garnet. The P-T path for the rocks indicates a prograde evolution, with peak P-T conditions of 3-5 kbar and approximately 700 °C. The metamorphic constraints and age presented in this paper enhance our understanding of the geological and tectonic evolution in SW Finland, coupling the Olkiluoto site to the Häme metamorphic and tectonic belt in Finland and highlighting tectonic and metamorphic similarities with the Ljusdal Block of Sweden.

1 Introduction

The tectonic evolution and the metamorphic record from the latter parts of Svecofennian orogeny has in the past been inferred to be similar in S Finland and central E Sweden (Hietanen, 1975; Korja and Heikkinen, 2005; Högdahl and Bergman, 2020; Engström et al., 2022). However, the coupling between these regions has been challenging to establish due to the prolonged tectonic evolution and the polymetamorphic nature of the Palaeoproterozoic bedrock, which often obscures the detailed P-T record for these rocks. Thus, novel geochronological techniques, particularly *in situ* Lu-Hf geochronology focusing on key metamorphic minerals like garnet, are indispensable for accurately delineating and investigating these ancient polymetamorphic terranes. Such approaches offer enhanced precision in constraining the timing of metamorphic events compared to traditional methodologies (Brown et al., 2022; Tamblyn et al., 2022; Simpson et al., 2023).

This study focuses on resolving the tectonic evolution in the Olkiluoto study area, which was affected by at least one, possibly two, significant metamorphic events during the Palaeoproterozoic Svecofennian orogeny (Tuisku and Kärki, 2010; Saukko et al., 2020). The Palaeoproterozoic bedrock of southern Finland consists to a large extent of granitoids and migmatites (e.g. Nironen, 2017). Based on lithological, geochemical and geochronological data, the Svecofennian crustal domain in Finland is divided into two major lithotectonic units: the Western Finland subprovince (WFS); and the Southern Finland subprovince (SFS) (Fig. 1; Korsman et al., 1997; Väisänen et al., 2002; Lahtinen et al., 2005; Nironen, 2017). The Svecofennian Province of Finland is separated from the Ljusdal lithotectonic unit in Central E Sweden (Högdahl and Bergman, 2020) by the Gulf of Bothnia. Despite this geographical separation, both regions show similar characteristics in terms of the rock types and structures (Fig. 1). These similar features are comparable in magmatic activity and structural evolution coupled with the same style and timing of metamorphism (e.g. Kähkönen, 2005; Nironen, 2005; Bergman et al., 2008; Väisänen et al., 2012; Högdahl and Bergman, 2020).

https://doi.org/10.5194/egusphere-2024-2034
Preprint. Discussion started: 15 July 2024

The Olkiluoto site is the location for the Finnish deep geological repository for spent nuclear fuel, and this study is part of the geological site characterisation. Our investigation provides new insights into the tectonic history of the Olkiluoto site and SW Finland during the Palaeoproterozoic Svecofennian orogeny (Fig. 1). The tectonic evolution has been defined through the analysis of garnet, a key mineral that serves as a reliable indicator of metamorphic conditions and thermal history within the crust**.** We have used the recently developed *in situ* Lu-Hf geochronology employing the use of laser ablation-inductively coupled tandem-quadrupole-mass spectrometry (LA-ICP-Q-MS/MS) (Brown et al., 2022; Simpson et al., 2021, 2023) to demonstrate that garnet and apatite in felsic, migmatitic tonalitic-granitic-granodioritic (TGG) intrusive rocks show metamorphism with one distinct metamorphic event and possibly an earlier event. Even though the Olkiluoto investigation area is small, the results of this study can be connected to a more regional context regarding the tectonic framework in southern Finland. The Lu-Hf geochronology from the Olkiluoto site combined with pressure-temperature modelling, provide new insight into how metamorphic processes and tectonic events were interconnected in S Finland. This knowledge is important for establishing connections with the Ljusdal lithotectonic unit in Central E Sweden. Recent studies by Engström et al., (2022); Lahtinen et al., (2023); Luth et al., (2024) infer that the coupling of the Olkiluoto area to Central E Sweden is plausible. However, more constraints and detailed research is required from adjacent areas in SW Finland and Central E Sweden to define the tectonic and metamorphic evolution and the coupling between these two areas.

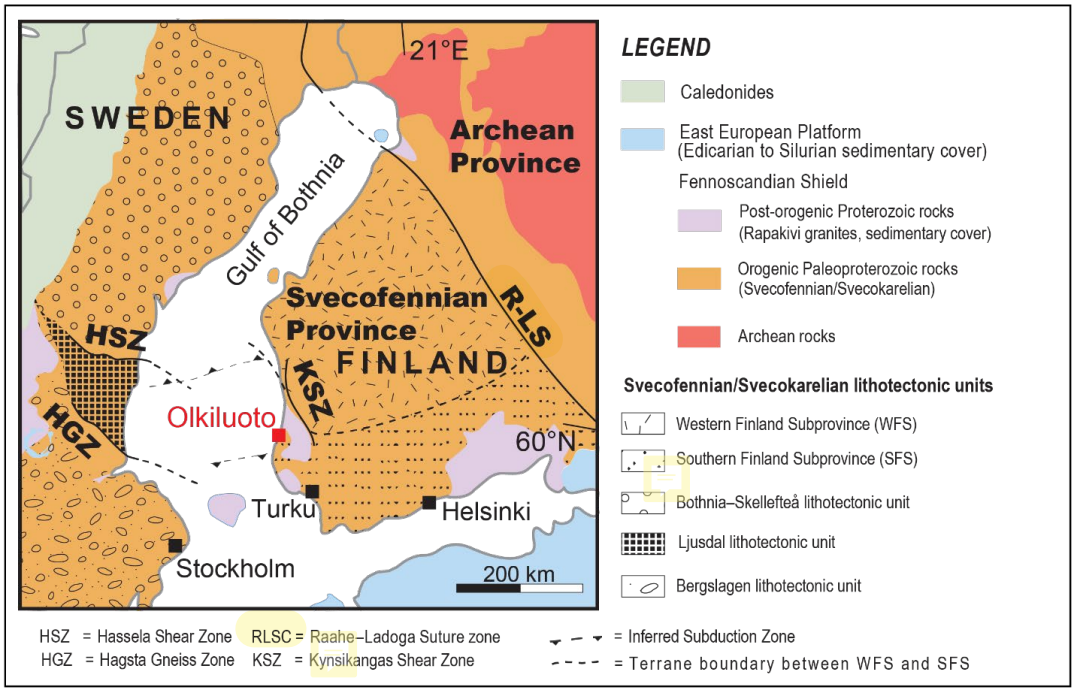

Figure 1. Geological map of the Fennoscandian shield. Olkiluoto is indicated with a red square. Map modified from Koistinen et al., 2001; Korja & Heikkinen, 2005; Nironen, 2017 and Stephens, 2020.

2 Geological setting of the study area

2.1 Tectonic framework

The Palaeoproterozoic Svecofennian orogeny, and its corresponding crustal province, were first introduced in the classic review by Gaál and Gorbatschev (1987) (Fig. 1). Since then, several tectonic models have been presented for

https://doi.org/10.5194/egusphere-2024-2034
Preprint. Discussion started: 15 July 2024

the evolution of the accretionary orogen (e.g. Nironen, 1997, Lahtinen et al., 2005, Lahtinen et al., 2023). The orogeny initiated from 1.92 Ga to 1.87 Ga (Nironen, 2017; Heilimo et al., 2023) with a collisional stage during which several volcanic arc complexes or microcontinents laterally accreted onto the margin of the Archean Karelia craton (e.g. Lahtinen et al., 2005). This convergence stage included several thrust sheets that developed within a W–SW to E–NE compressional environment in southern Finland (Nironen, 2017; Torvela & Kurhila, 2020). In the Western Finland Subprovince (WFS), moderate crustal thickening led to widespread development of granites and associated migmatites, with peak metamorphism occurring at 1.88-1.87 Ga (Mäkitie et al., 2012; Chopin et al., 2020). The subsequent tectonic phases included minor crustal extension, followed by the next step of orogenic convergence that resumed at ca. 1.84 Ga and especially in S Finland initiated a younger metamorphic event forming granites and associated migmatites (Lahtinen et al., 2005; Torvela et al., 2008; Torvela and Kurhila, 2020; Kara et al., 2021). This transpressional deformation phase was characterized by intensive folding and shear zone development (Väisänen et al., 2002; Väisänen and Skyttä, 2007; Torvela and Kurhila, 2020).

The Svecofennian orogeny is characterized by two main high-T/low-P type metamorphic events. The first event occurred at 1.88–1.87 Ga, reaching upper amphibolite facies, and can be detected throughout the Finnish Svecofennian (Korsman et al., 1999; Nironen, 2017). The later event at 1.84–1.80 Ga involved high-T metamorphism to granulite facies in large areas of southernmost Finland and was associated with emplacement of granites together with anatectic melting resulting in the formation of migmatites and pegmatites during the late stages of the Svecofennian orogeny (Korsman et al., 1999; Väisänen and Hölttä, 1999; Väisänen et al., 2002; Skyttä and Mänttäri, 2008). Similar metamorphic ages and styles occur in the Ljusdal lithotectonic unit, central E Sweden (Högdahl and Bergman, 2020) (see Fig. 1). The rocks within the Ljusdal lithotectonic unit were intruded by the Ljusdal Batholith at ca. 1.86-1.84 Ga (Högdahl et al., 2008) and were affected by polyphase, ductile deformation, coupled to two episodes of high-grade, low-pressure metamorphism during the Svecofennian orogeny, dated at ca. 1.85 Ga and 1.83-1.82 Ga, with prolonged crustal heating continuing to at least 1.80 Ga (Högdahl et al., 2008; Högdahl and Bergman, 2020). The Olkiluoto site has been deduced to exhibit a similar tectonic evolution and metamorphic signatures as the Ljusdal lithotectonic unit in central E Sweden (Högdahl et al., 2008; Engström et al., 2022).

2.2 Geology of the Olkiluoto area

Engström et al., (2022) defined that the Olkiluoto site experienced a tectonic evolution where ductile deformation took place in several steps, coinciding with the formation of migmatites and leucosomes under high-T conditions in the Palaeoproterozoic crust. Thus, the bedrock at Olkiluoto island consists of Palaeoproterozoic, mostly intrusive and supracrustal rocks and is situated in the westernmost part of the Southern Finland subprovince (Fig. 1 and Fig. 2). The felsic, tonalitic-granitic-granodioritic (TGG) intrusive rocks are migmatised with small, injected veins of pegmatitic-granitic (PGR) leucosome. Since this TGG intrusive rock is less deformed and altered by the subsequent polyphase ductile deformation events compared to the metapelitic migmatitic rocks (Engström et al., 2022), it is well suited for our study on the metamorphic evolution in Olkiluoto. The bedrock at the site is also intruded by diabase dykes, likely of Mesoproterozoic age. The migmatites in Olkiluoto are divided into two main groups: vein- and dyke-structured metatexites (VGN in Fig. 2); and nebulitic diatexites (DGN in Fig. 2), which can be further subdivided into several subtypes on the basis of their migmatite structures (Kärki, 2015). Metatexitic migmatites dominate the western part of the island, whereas diatexites are abundant in the eastern part of the island (Fig. 2).

Earlier studies indicate that two distinct metamorphic events occurred in Olkiluoto (Tuisku and Kärki, 2010; Saukko et al., 2020; Engström et al., 2022), with the metamorphic conditions of the first event estimated to have a peak pressure of approximately 6 kbar. This earlier event is interpreted due to some samples producing a higher estimated peak pressure than the average metamorphic grade (3-4 kbar), and was inferred to be connected to magmatic processes and emplacement of the protolith of TGG rocks (Tuisku and Kärki, 2010). The mineral assemblages of the second metamorphic peak are indicative of upper amphibolite facies, ~~with calculated P-T conditions~~ at 660–700 ºC and 3.7 – 4.2 kbar (Tuisku and Kärki, 2010). The timing of these events are constrained using tectonic events and metamorphic

https://doi.org/10.5194/egusphere-2024-2034
Preprint. Discussion started: 15 July 2024

U-Pb zircon ages at ca. 1.87–1.84 Ga and 1.82–1.78 Ga (Engström et al., 2022). The pressure difference of approximately ~~two~~ kbar between the two metamorphic stages indicate either an erosion phase between the metamorphic phases or a significant crustal uplift. The latter metamorphic event is characterized by injected granitic and pegmatitic leucosome veins and dykes that are crosscutting the earlier generated foliation (Engström et al., 2022).

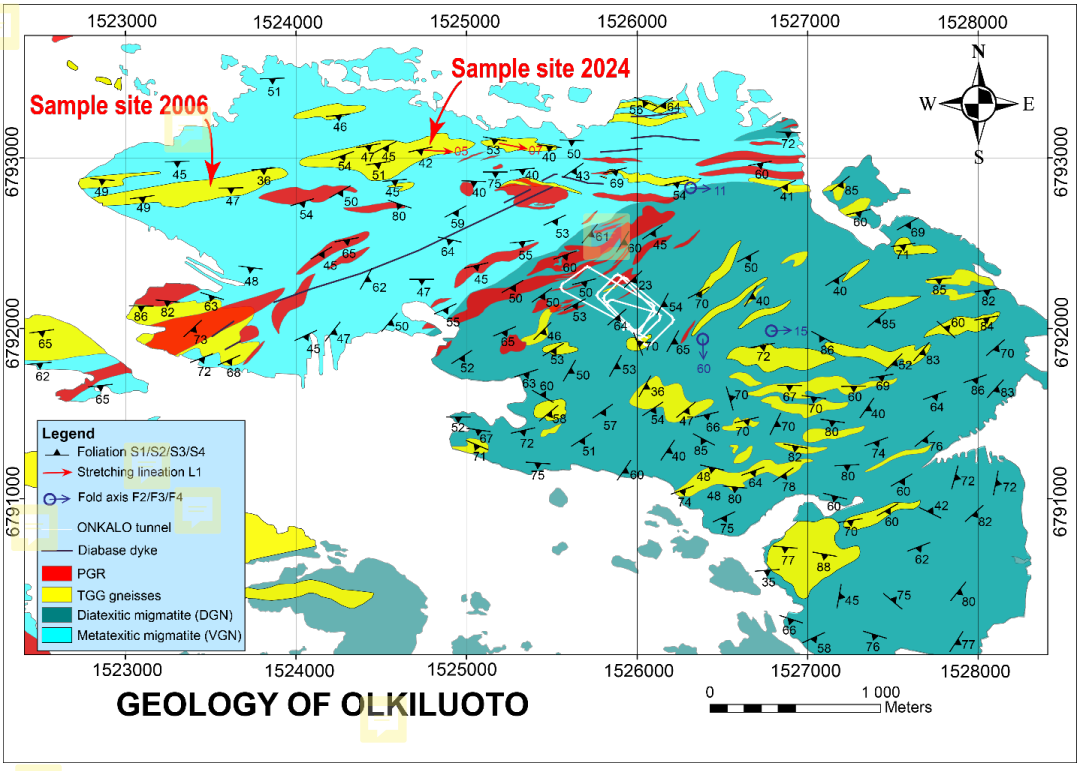

Figure 2. Geological map of Olkiluoto (modified from Aaltonen et al., 2016 and Engström et al., 2022). The locations of the investigated outcrops in 2024 and 2006 are also indicated.

3 Methods of the study

This study includes whole rock geochemistry of the different lithological units at the site coupled with a detailed outcrop study ~~on~~ the TGG intrusive rock representing the protolith ~~for the first metamorphic phase~~ in Olkiluoto (Engström et al., 2022). ~~The detailed outcrop study includes structural geological mapping~~, thin sections and micro-XRF images. ~~The~~ study ~~was performed on a single~~ outcrop (see Fig. 2, sample site 2024) ~~where~~ two ~~bedrock pieces~~ (approx. 50 cm x 10 cm x 8 cm) were ~~sawed out and~~ further investigated ~~(~~Fig. 3). Both samples, MM30 and MM31 (Fig. 3) are compositionally similar, containing large subhedral garnet crystals up to 3-5 cm in size in leucosomes and small anhedral garnet crystals within the matrix up to 0.3-0.7 cm in size. Finally, garnet and apatite grains were selected from these samples for ~~detailed~~ analysis.

https://doi.org/10.5194/egusphere-2024-2034
Preprint. Discussion started: 15 July 2024

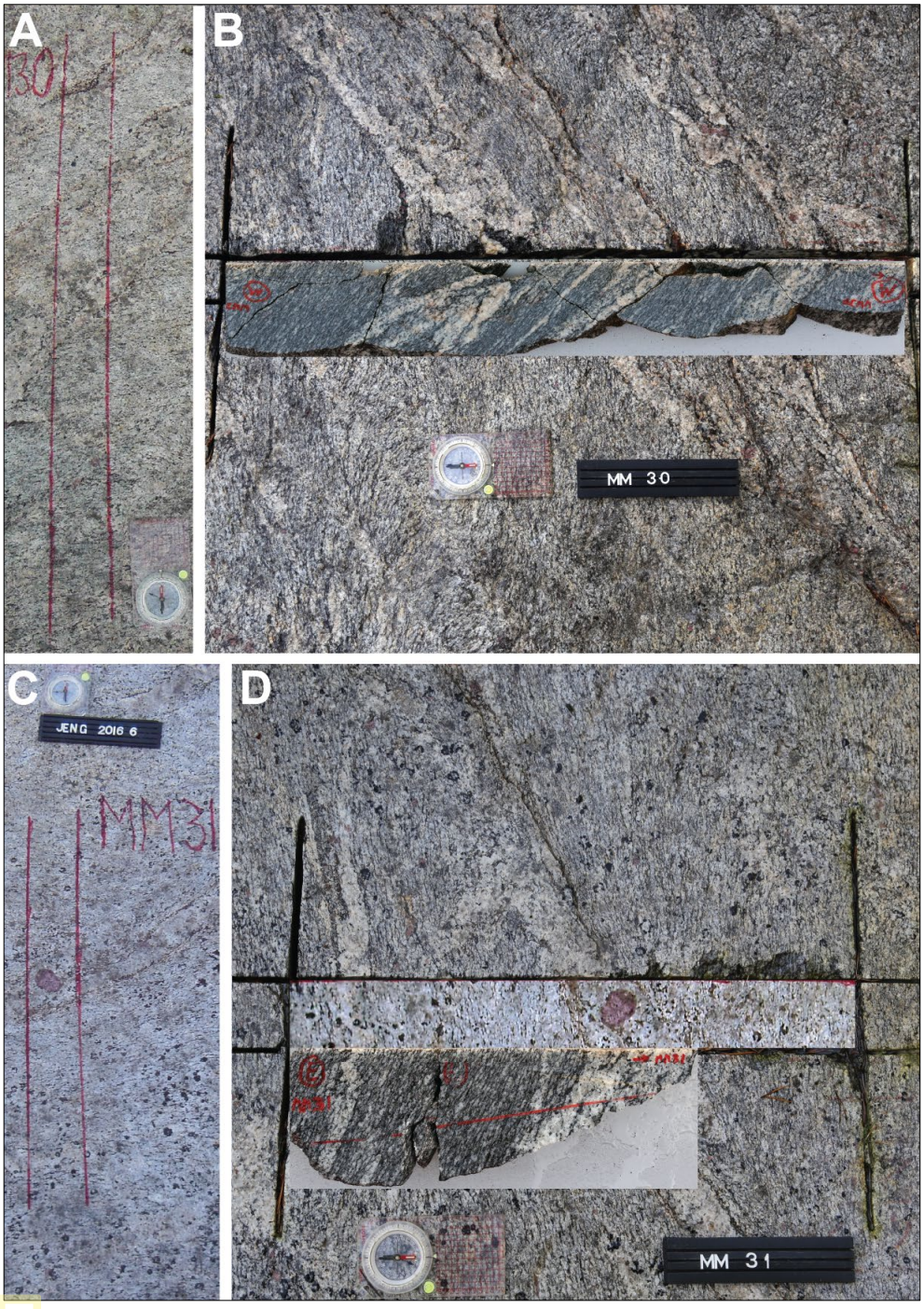

130 **Figure 3.** The TGG outcrop indicating the sawed-out rock sample areas. Sample area MM30, with view from the top (A) and with cut-out (B). Sample area MM31, with view from the top (C) and with cut-out (D).

https://doi.org/10.5194/egusphere-2024-2034
Preprint. Discussion started: 15 July 2024

3.1 Sample description

The TGG rocks ~~found~~ in the NW part of the Olkiluoto site have been least affected by the different polyphase ductile deformation events. The rocks are pale-grey in colour and contain a ~~metamorphic~~ banding with a prominent stretching lineation. Garnet occurs as small grains scattered in the matrix and as large grains that occur within leucosomes. Both types of garnet were targeted in this study to determine if ~~these garnets~~ grew during single or multiple phases of metamorphism. The small garnet grains (up to 0.7 cm) (Fig. 3A-B) were removed from ~~one sawed~~ sample by slicing ~~the sample using a~~ small saw and then cutting out the small grains where they were observed. Three small grains were then mounted in a single epoxy mount. The large grain was embedded in the leucosome (ca. 5 cm) of sample MM31 (Fig. 3C-D) and was removed by sawing and then cut in half in order to fit the 2.5 cm epoxy mount. The mineralogy ~~in~~ the rock consists of quartz, K-feldspar, plagioclase, biotite and garnet, with accessory apatite and cordierite, which often exhibit pinite alteration. The rocks are coarse grained, with K-feldspar grains up to 1 cm and plagioclase and quartz of up to 0.5 cm. The grain size in the leucosome is larger, with K-feldspar, quartz and garnet up to several cm in size. Garnet grains in both the matrix and leucosomes have cores rich in quartz inclusions, often seeming to define a symplectitic-like texture. Rarely, biotite is also observed in garnet cores. Apatite inclusions commonly occur on the outer edge of the core domain and in the rims. Garnet rims are generally inclusion-poor, but where inclusions occur, they are large and usually consist of quartz, apatite, biotite or K-feldspar. Garnet grains are subhedral with irregular grain boundaries, often with embayments. The matrix foliation is defined by biotite, which forms elongate grains up to several mm in size. Biotite is generally also slightly coarser in the leucosomes and the foliation is not as well defined with biotite grains often wrapping around large garnet grains. In both the matrix rocks and the leucosome, biotite grains are subhedral, often having scalloped grain edges. K-feldspar, quartz and plagioclase all have irregular grain boundaries, with scalloped edges, they occur as rounded inclusions in each other, and form thin, film-like segregations. Larger grains are often elongate and oriented parallel to the foliation of the sample.

3.2 Method description – mineral chemistry

One large garnet (5 cm) was cut in half and mounted in epoxy, while a second large garnet from the sample was prepared as a thin section. Three of the smaller garnets were made into an epoxy mount, and several regions with smaller garnets were prepared as thin sections. The epoxy mounts were imaged using a Bruker Micro-XRF M4 Tornado hosted at the Geological Survey of Finland (GTK). The system is equipped with a 30-Watt rhodium (Rh) anode X-ray tube, two 30 mm^2 silicon drift detectors (SDD) with an energy resolution of < 145 eV (MnKα) at 275 kcps (kilocounts per second) via beryllium windows and poly-capillary optics. All data acquisition was performed with an accelerating voltage of 50 kV, a beam current of 500 µA using a fixed spot size of 20 µm under a 2 mbar vacuum. The samples were measured in one single run using a step size of 40 µm and a pixel dwell time of 20 ms/pixel. The qualitative elemental maps were generated using the Bruker M4 software with later processing in XMapTools (Lanari et al., 2014).

Quantified chemical analysis were obtained with a CAMECA SX100 electron microprobe analyzer (EMPA) at GTK using the WDS (wavelength-dispersive) technique. Accelerating voltage and beam current were set to 15kV and 15nA, respectively. A defocused beam diameter of 5 µm was used for the spot analysis. Analytical results have been corrected using the PAP on-line correction program (Pouchou and Pichoir, 1986). Natural minerals and synthetic metals were used as standards.

https://doi.org/10.5194/egusphere-2024-2034
Preprint. Discussion started: 15 July 2024

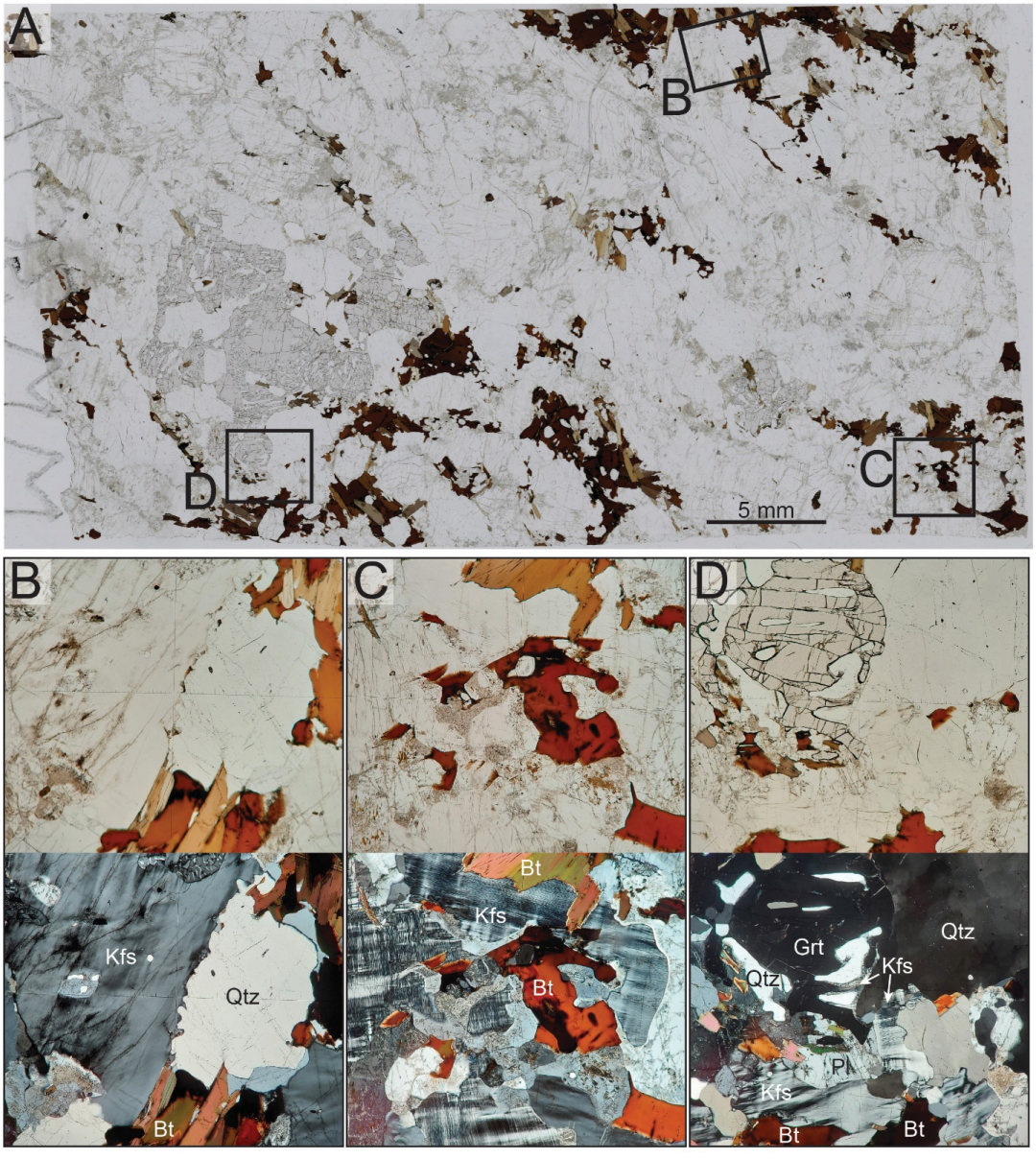

Figure 4. Sample photomicrographs. A. Plane polarised image of thin section for sample MM30 with the location of images shown in B-D as plane and cross polarised images. B. K-feldspar and quartz grains showing irregular grain boundaries. C. Biotite grains with scalloped edges, finer grained intergrowths of K-feldspar and plagioclase. D. Edge of garnet grain with thin films of K-feldspar.

https://doi.org/10.5194/egusphere-2024-2034
Preprint. Discussion started: 15 July 2024

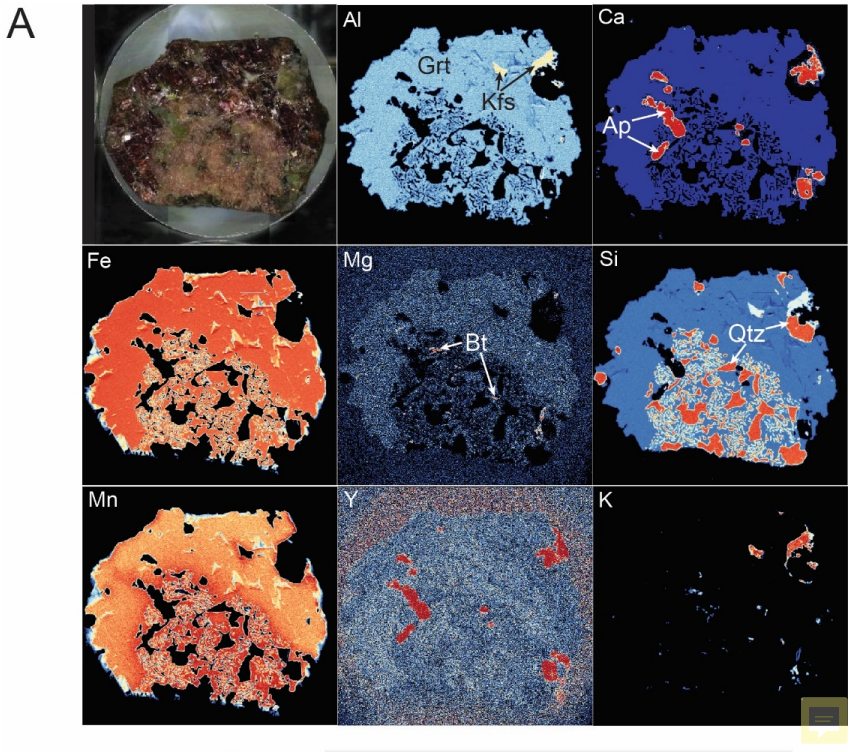

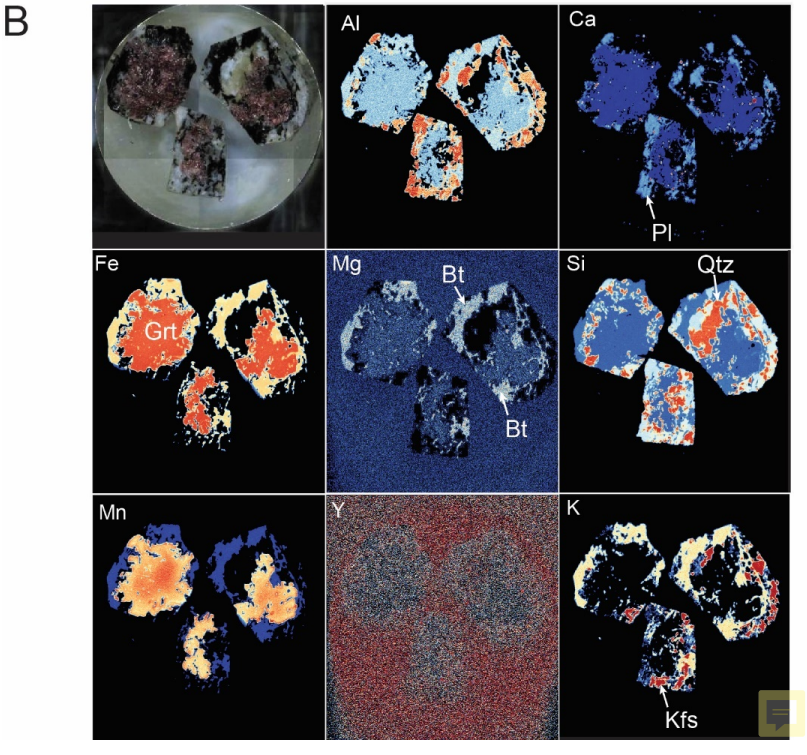

https://doi.org/10.5194/egusphere-2024-2034
Preprint. Discussion started: 15 July 2024

Figure 5. A. Garnet from leucosome mounted in epoxy with elemental images of the mount obtained by micro-XRF. Images are intensity maps with the colour scale varying from black-blue (low) to red (high). B. Garnet grains from the matrix mounted in epoxy with elemental images of the mount obtained by micro-XRF. Images are intensity maps with the colour scale varying from black-blue (low) to red (high).

3.3 Method description – garnet and apatite Lu-Hf geochronology

Two garnet-bearing samples (one leucosome and one with matrix garnet) were prepared into 2.5 cm polished epoxy mounts (Fig. 5) for *in situ* Lu-Hf geochronology at Adelaide Microscopy, University of Adelaide, Australia. Garnet and apatite Lu-Hf dating was conducted over two analytical sessions using a RESOlution-LR 193nm excimer laser ablation system, coupled to an Agilent 8900 ICP-MS/MS. The laser beam diameter was set to 173 µm (garnet) and 120 µm (apatite), and ablation was conducted at 10 Hz repetition rate and a fluence of ~3.5 J/cm^2.

The laser-based Lu-Hf method uses a NH_3 – He gas mixture in the reaction-cell of the mass spectrometer to promote high-order reaction products of Hf, with a mass-shift of +82, while equivalent Lu and Yb reaction products are minimal (i.e., Hf reacts at a rate of 50-60% while Lu reaction is < 0.003%; Simpson et al., 2021). Consequently, the resulting mass-shifted (+82 amu) reaction products of $^{176+82}$Hf and $^{178+82}$Hf can be measured free from isobaric interferences. ^{177}Hf was subsequently calculated from ^{178}Hf, assuming natural abundances. ^{175}Lu was measured on-mass as a proxy for ^{176}Lu (see details in Simpson et al., 2021, 2023). In addition to Lu and Hf isotopes, other trace elements including a selection of other Rare Earth elements (REEs) (details in Supplementary Table) were measured simultaneously to monitor for inclusions and to characterise the nature of the fluids. However, not every REE was measured as this would compromise the dwell times on the Hf isotopes required for age calculations. For garnet, the reference material Hogsbo garnet was analysed repeatedly to correct for matrix-dependent fractionation (Simpson et al., 2021; Glorie et al., 2024b) and secondary garnet reference material BP-1 (Black Point, South Australia; Glorie et al., 2024b) was used to validate the accuracy of the Lu-Hf dates. BP-1 produced a garnet Lu-Hf isochron age of 1749 ± 15 Ma (Supplementary Table), which is consistent with the published monazite U-Pb age of 1745 ± 14 Ma (Lane, 2011).

For apatite, the reference material OD-306 was analysed repeatedly to correct for matrix-dependent fractionation (1597 ± 7 Ma; Thompson et al., 2016). The secondary reference apatites Bamble-1 (Bamble sector, SE Norway; Lu-Hf age of 1102 ± 5 Ma; Glorie et al., 2024a) and HR-1 (Harts Range, NT Australia; Lu-Hf age: 343 ± 2 Ma; Glorie et al., 2022) were used to monitor accuracy. During this study the age obtained for Bamble-1 was 1084 ± 18 Ma and for HR-1 was 344 ± 3 Ma (Supplementary Table).

Apatite U-Pb and trace element analysis was conducted on the same instrumentation as for the Lu-Hf analyses, using identical analytical parameters as in Gillespie et al., (2018) and Glorie et al., (2019), including a laser diameter of 30µm and repetition rate of 5Hz. The primary reference material used was MAD (ID-TIMS U-Pb age 473.5 ± 0.7 Ma; Thomson et al., 2012; Chew et al., 2014). 401 apatite was used as a secondary standard, producing a weighted mean ^{206}Pb/^{238}U age of 529 ± 2 Ma (Supplementary Table). This is in good agreement with the published age (ID-MC-ICP-MS U-Pb age 530.3 ± 1.5 Ma; Thompson et al., 2016).

Isotope ratios and trace element concentrations were calculated in LADR (Norris and Danyushevsky, 2018) using NIST 610 as a primary standard (Nebel et al., 2009). Lu-Hf ages were calculated as inverse isochrons using IsoplotR (Vermeesch, 2018; Li and Vermeesch, 2021) with the ^{176}Lu decay constant of Söderlund et al., (2004); 0.0001867 ± 0.00000008 Ma^{-1}. For samples that produced exclusively high-radiogenic ^{177}Hf/^{176}Hf ratios (< ~0.1), the isochron was anchored to an initial ^{177}Hf/^{176}Hf composition of 3.55 ± 0.05, which spans the entire range of initial ^{177}Hf/^{176}Hf ratios of the terrestrial reservoir (e.g. Spencer et al., 2020).

https://doi.org/10.5194/egusphere-2024-2034
Preprint. Discussion started: 15 July 2024

3.4 Method description – Pressure-temperature pseudosection modelling

Pressure-temperature pseudosections were calculated for sample MM30A using the software package Theriak/Domino (Capitani and Petrakakis, 2010) and the database of Holland and Powell, (2011) for the geologically realistic system MnNCKFMASH (MnO-Na_2O-CaO-K_2O-FeO-MgO-Al_2O_3-SiO_2-H_2O).

The 'metapelite set' of models from White et al., (2014a), converted to Theriak-Domino format by Doug Tinkham (see Jørgensen et al., 2019) were applied. These are White et al., (2014b) for orthopyroxene, garnet, biotite, staurolite, chloritoid, cordierite and chlorite; White et al., (2014a) for muscovite and silicate melt; Holland and Powell, (2011) for epidote; Holland and Powell, (2003) for plagioclase; quartz, H_2O, kyanite, sillimanite and andalusite are also included as pure phases. Due to the large amount of Mn present in the garnet, MnO was included in the system. However, the low Ti content and absence of Ti bearing minerals makes the inclusion of TiO_2 unnecessary. Additionally, a lack of Fe^{3+} bearing phases such as magnetite and the low indicated Fe^{3+} contents in recalculated garnet analysis (see supplementary Table) indicated that including ferric iron in the modelling was unnecessary.

The presence of leucosomes, fine-grained domains and cuspate grain boundaries in the rock suggest that melt was part of the peak assemblage of the samples. Since it is impossible to know if this melt was retained in the system, a T-X_{H2O} diagram was calculated to indicate an appropriate H_2O value for the P-T diagram (Supplementary Fig. S1).

Many thin sections contain a significant amount of apatite, which is also observed as inclusions within garnet (Fig. 5A). Since apatite contains appreciable amounts of CaO, a T-X_{CaO} diagram was also generated using the measured amount of P_2O_5 to determine the maximum amount of CaO that could be attributed to apatite (Supplementary Fig. S2).

4 Results

4.1 Whole-rock geochemistry

To further support metamorphic constraints, 118 whole-rock geochemical analyses of the Olkiluoto site TGG were compiled from Aaltonen et al., (2016) including metatexites and diatextites, as well as injected pegmatitic granites and leucosome veins. The Olkiluoto region diabase dykes have been excluded from the dataset. Figure 6 shows the main whole-rock compositional characteristics of the Olkiluoto site rocks, distinguishing between normal TGGs and high-P TGGs. Geochemical discrimination diagrams such as TAS, show the difference between normal dominant TGGs (SiO_2 49.60-77.83 wt. % and P_2O_5 0.10-0.23 wt. %) and high-P TGGs (SiO_2 48.45-67.57 wt. % and P_2O_5 0.31-1.73 wt. %) (Fig. 6). In addition, AFM-diagrams effectively illustrate this distinction with high-P TGGs following the tholeiitic series trend, indicative of an older protolith part of migmatites with mainly lower SiO_2 contents, and most of the TGGs following a calc-alkaline series trend typical for arc environments fitting well to Svecofennian orogeny.

https://doi.org/10.5194/egusphere-2024-2034
Preprint. Discussion started: 15 July 2024

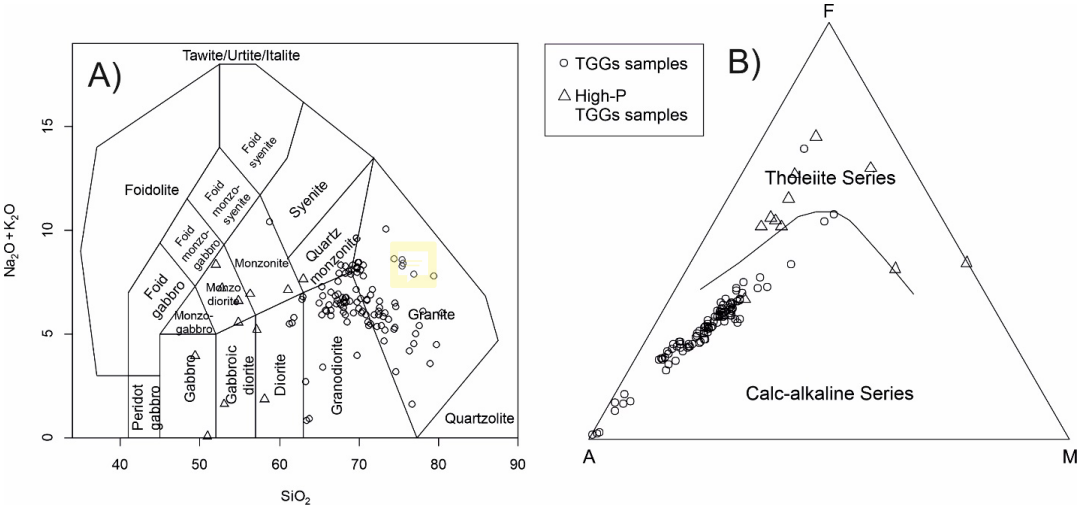

Figure 6. The whole-rock geochemistry from Olkiluoto region. A. TAS diagram after Middlemost (1994). B. AFM diagram after Irvine and Baragar (1971). Lithologies: dominant TGG = tonalitic-granitic-granodioritic migmatites including metatexites and diatexites, and high-P TGGs.

4.2 Mineral chemistry

The garnet mineral chemistry indicates significant iron enrichment, with X_{Alm} (=Fe/(Fe+Mn+Mg+Ca)) of 0.77 to 0.80. In the large garnet grains, X_{Alm} is fairly constant across the grain, with slight increases next to quartz inclusions. In the small garnet grains, X_{Alm} is slightly elevated in the core and also the rim (Fig. 7B). X_{Pyr}(=Mg/(Fe+Mn+Mg+Ca)) values range between 0.08 to 0.12, with the lowest values found in grain cores (0.08) and directly adjacent quartz inclusions. The highest X_{Pyr} values (0.12) are from the grain rim, although right at the edge of the grain, the X_{Pyr} content drops abruptly (Fig. 7B, D). The same patterns are observed in both large and small garnet grains (Fig. 7). X_{Sps}(=Mn/(Fe+Mn+Mg+Ca)) values vary from 0.11 to 0.08 with the higher values coming from the grain core, directly adjacent to quartz inclusions and at the grain (Fig. 7). A similar pattern is observed in both, large and small garnet grains (Fig. 7). X_{Grs} (=Ca/(Fe+Mn+Mg+Ca)) values exhibit flat profiles in both large and small garnet grains, with a constant value of just over 0.02. The micro-XRF maps indicate similar compositional variations, with mostly uniform Fe, Mg and Ca (Fig. 5). The Mn maps have higher core values, higher values around quartz inclusions and on the rim of grains. The Y map of the large garnet clearly shows the location of high Y apatite inclusions, which are mostly hosted at the rims of large garnet grains (Fig. 5A). The larger garnet seems to have higher Y contents, particularly in the rim zone, although this may be due to a significant amount of quartz inclusions in the garnet core (Fig. 5A). The small garnets appear to be uniformly low in Y content (Fig. 5B).

Biotite grains have X_{Mg}(=Mg/(Mg+Fe)) values of 0.34 to 0.37, with higher values observed in grains included in garnet. TiO_2 content varies from 1.84 to 2.88 wt%. In the large garnet sample, plagioclase exhibits a variable composition with X_{Ab}(=Na/(Na+Ca+K)) of 0.76 to 0.96. The sample with small garnet has a more restricted X_{Ab} of 0.74-0.79. K-feldspar is dominantly K-rich with X_K(=K/(Ca+Na+K)) of 0.81 to 0.87 in both, the small and large garnet samples.

https://doi.org/10.5194/egusphere-2024-2034
Preprint. Discussion started: 15 July 2024

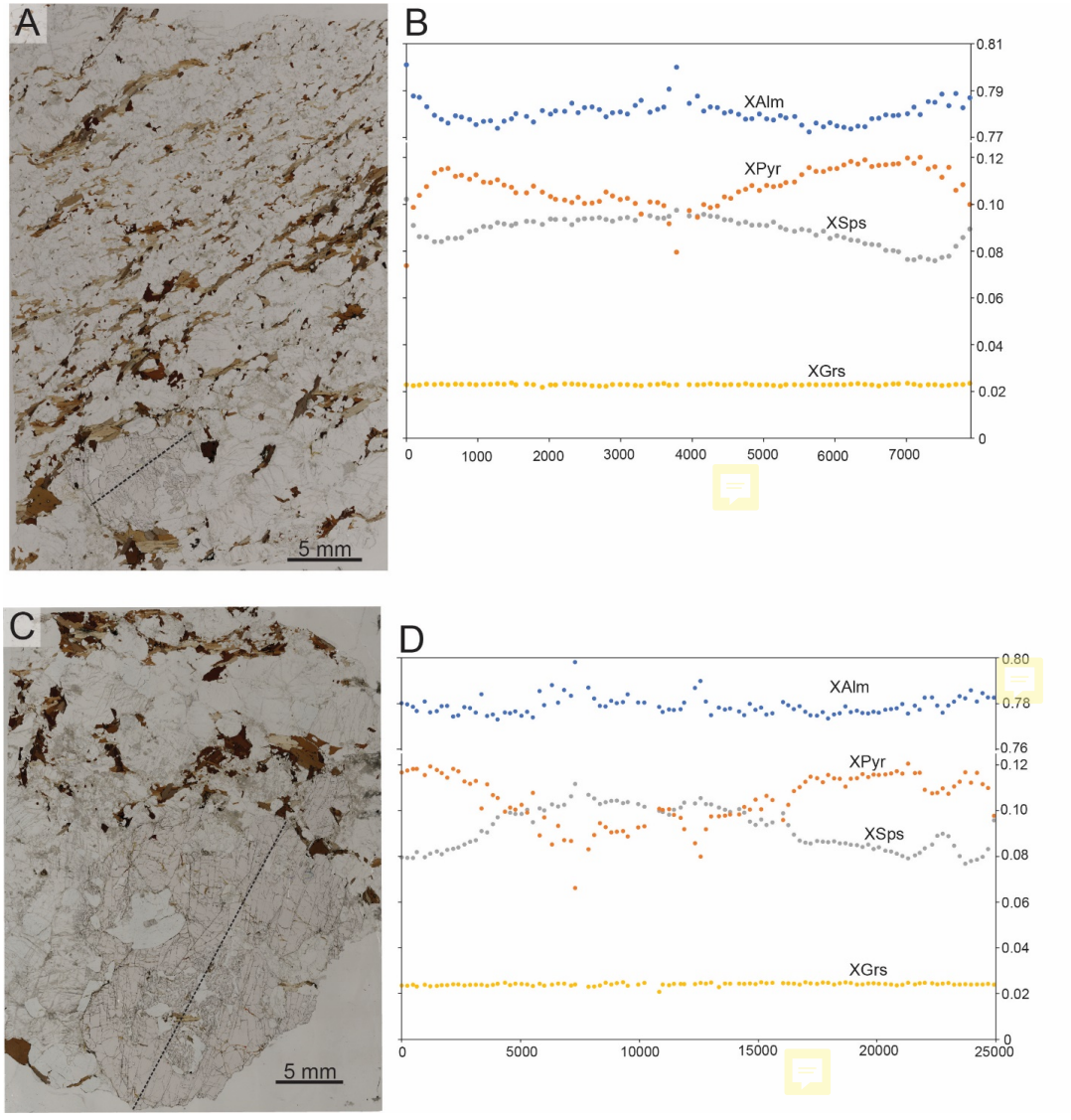

Figure 7. Garnet major element zonation. A. Plane polarised image of a thin section of the matrix domain including the location of a small garnet grain used for the EPMA travers. The location of the traverse is indicated with the thin dashed line. B. Garnet traverse for the grain in Fig. 7A. The traverse starts from the left side of the garnet grain. C. Plane polarised image of a thin section from the leucosome with a large garnet grain. The location of the traverse is indicated with the thin dashed line. D. Garnet traverse for the grain in Fig. 7C. The traverse starts from the left side of the garnet grain.

https://doi.org/10.5194/egusphere-2024-2034
Preprint. Discussion started: 15 July 2024

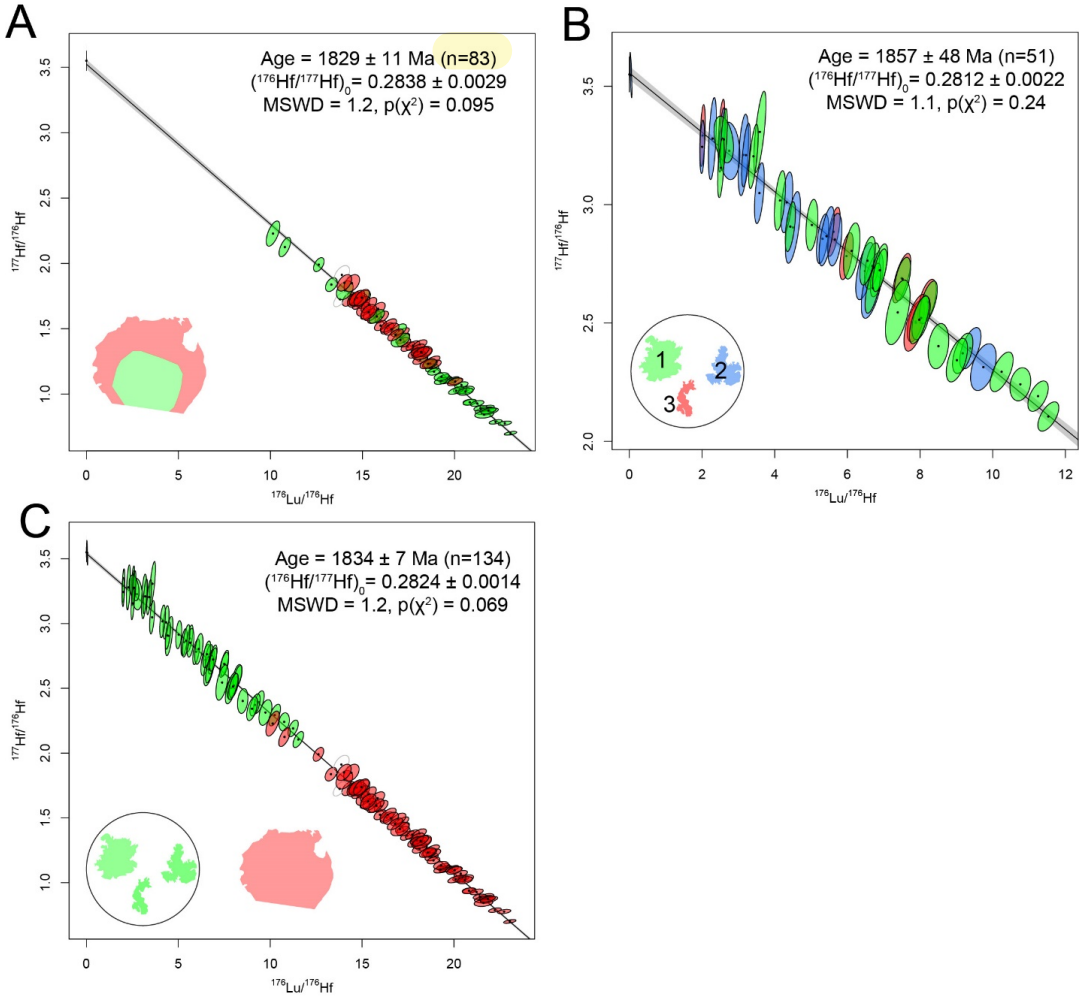

Figure 8. A. Lu-Hf inverse isochron for the large garnet sample. Analyses are coloured based on their location within the garnet grain (green=core, red=rim). B. Lu-Hf inverse isochron for the small garnet sample. Analyses are coloured based on which garnet grain they were obtained from (see inset for colour key). C. Lu-Hf inverse isochron of both samples plotted together (red analyses correspond to the large garnet grain and green analyses correspond to the small garnet grains).

4.3 Garnet Lu–Hf Geochronology

Two garnet samples were targeted for Lu-Hf geochronology. One large garnet hosted in a leucosome and three small grains obtained from the matrix. From the large grain, a total of 84 analyses were conducted with 42 targeting the grain core and 42 at the grain rim (see Supplementary Fig. S3 for spot locations). Two analyses were excluded from age calculations due to the presence of inclusions. When all data is plotted on an isochron anchored to an initial $^{177}Hf/^{176}Hf$ ratio of 3.55 ± 0.05 (covering the range of terrestrial values; Mark et al., 2023) the result is an isochron age of 1829 ± 11 Ma (n=83, MSWD = 1.2; Fig. 8A). Analyses obtained from the grain core have a larger spread in $^{176}Lu/^{176}Hf$ ratios yielding an age of 1828 ± 11 Ma (n=43, one analysis was duplicated with different segments of the signal selected; Supplementary Fig. S4), whereas the measurements from the garnet rim data give an identical isochron age with a larger uncertainty: 1828 ± 21 Ma (n=40, two data points were excluded due to inclusions,

https://doi.org/10.5194/egusphere-2024-2034
Preprint. Discussion started: 15 July 2024

Supplementary Fig. S5). Garnet cores have Lu contents of 10 to 70 ppm (average is 35 ppm) when calibrated to an internal standard of 12 wt% Al. Garnet rims have Lu contents of 10 to 25 ppm (average is 18 ppm).

The small garnet grains were targeted with 51 analyses in total (see Supplementary Fig. S6 for spot locations) and have a restricted $^{176}Lu/^{176}Hf$ ratio range, resulting in an anchored isochron age of 1857 ± 48 Ma (n=51; MSWD = 1.1; Fig. 8B). If the grains are plotted separately, they all produce the same age within ~~error,~~ but due to the smaller number of analyses the errors are larger. The small garnets have Lu contents ranging from 10 ppm to below the detection limit (average is 4 ppm). If all the garnet data is plotted together and anchored to an initial $^{177}Hf/^{176}Hf$ ratio of 3.55 ± 0.06, an isochron age of 1834 ± 7 Ma (n=134; MSWD = 1.2; Fig. 8C) can be produced.

4.4 Apatite Lu-Hf and U-Pb Geochronology

Apatite was dated using both Lu-Hf and U-Pb methods in two separate analytical sessions. The Lu-Hf data are mostly highly radiogenic (38 of 47 analyses with $^{177}Hf/^{176}Hf$ ratios <0.1) and define an anchored Lu-Hf isochron age of 1782 ± 10 Ma (MSWD = 1.5; Fig 9A). Alternatively, calculating a weighted mean common-Hf corrected Lu-Hf age (for apatites with $^{177}Hf/^{176}Hf$ ratios <0.1) returns an identical age within uncertainty of 1784 ± 8 Ma (MSWD = 1.3, n=38). The apatite REE spidergrams indicate slightly enriched light REEs, a pronounced negative Eu anomaly and flat HREE profiles. Based on the classification plot of O'Sullivan et al., (2020) the Olkiluoto ~~apatites are partial melts/leucosomes/high-grade metamorphic~~. The apatite U-Pb data plot on a linear trend with some slight scatter. An isochron based on 40 out of 45 analyses produces an isochron age of 1778 ± 16 Ma (MSWD = 0.41). The 5 analyses excluded from this isochron could be related to partial inheritance from an older event or isotopic disturbance (U-loss; Fig. 9B).

4.5 Pressure-temperature pseudosection modelling

For sample MM30A, the T-X_{H2O} diagram (supplementary material Fig. S5) indicates that the interpreted peak assemblage ~~field for these samples~~ of garnet + plagioclase + K-feldspar + biotite + quartz + melt is present at more elevated H_2O contents (>0.25 on the binary diagram). For this reason, H_2O was set at 0.3 for further calculations corresponding to a H_2O content of less than 1 wt%. In the T-X_{CaO} diagram, the interpreted peak assemblage ~~field~~ occurs only on the right side of the diagram suggesting that only a modest amount of CaO needs to be removed to account for apatite in the sample. The compositional isopleths of garnet ~~that are consistent with the garnet composition of the sample~~ also indicate only a small reduction in CaO, thus the P-T diagram for sample MM30A was calculated at 0.75 of the T-X_{CaO} diagram (indicating that of a total 100% CaO that could be attributed to apatite, only 25% was).

The P-T diagram for sample MM30A has the interpreted peak assemblage field of garnet + plagioclase + K-feldspar + biotite + quartz + melt present over a large range of pressures and temperatures, extending from 2.5 kbar to over 10 kbar and from 650 °C to 800 °C (Fig. 10). The garnet compositional isopleths which correspond to the garnet compositional range observed in the sample (X_{Alm}: 0.8-0.78; X_{Pyr}: 0.12-0.1; X_{Sps}: 0.1-0.08; X_{Grs}<0.04) occur in the lower pressure part of the field with compositional overlap occurring in the range of 3-5 kbar and ca. 700 °C (Fig. 10).

https://doi.org/10.5194/egusphere-2024-2034
Preprint. Discussion started: 15 July 2024

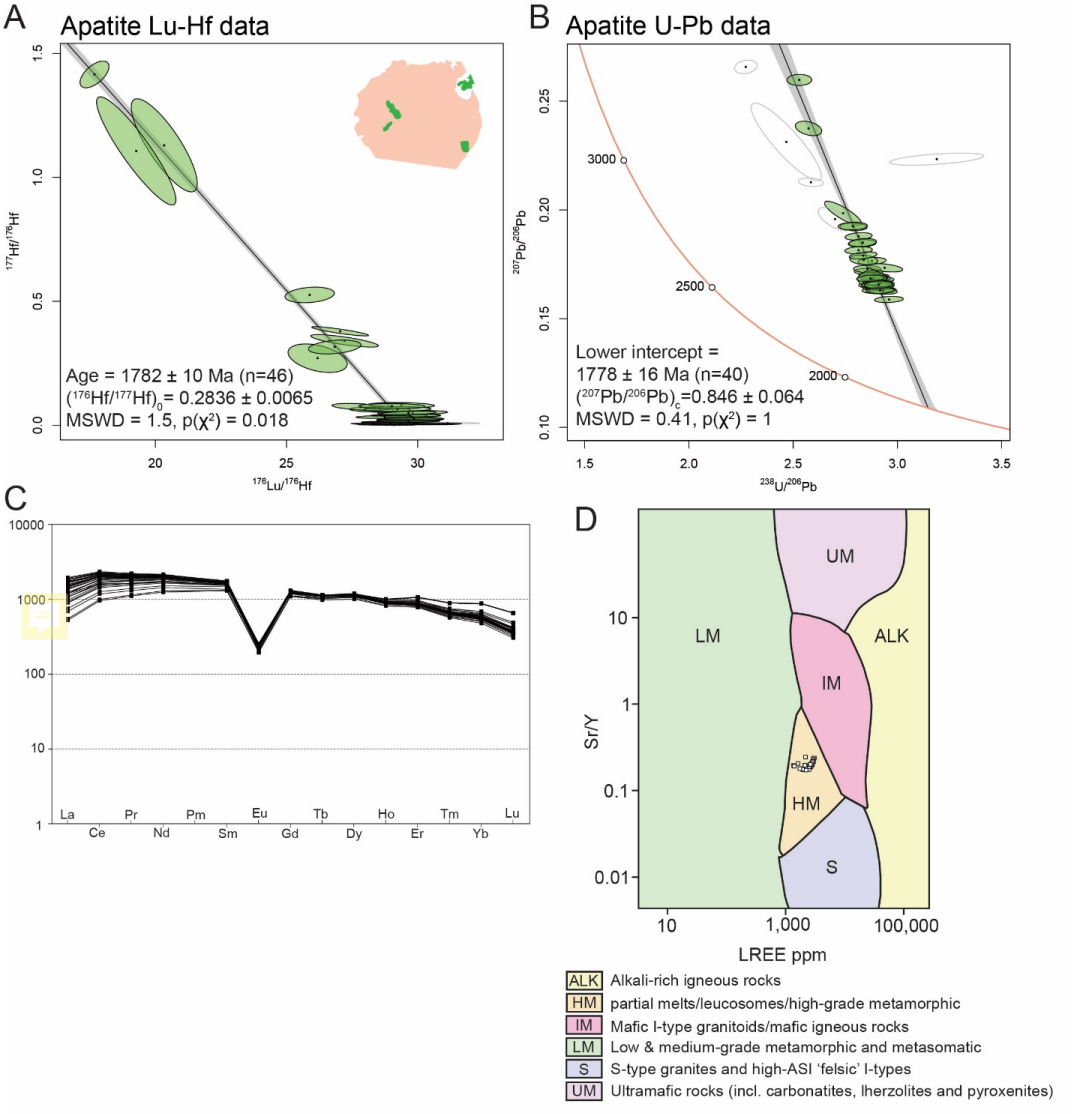

Figure 9. A. Lu-Hf inverse isochron for apatite occurring within the large garnet grain (green grains in the inset image). B. Apatite U-Pb data plotted on a Terra-Wasserburg concordia plot. C. Apatite REE spidergram normalised to chondrite (McDonough and Sun, 1995). D. Apatite classification biplot of O'Sullivan et al., (2020) based on Sr/Y vs ΣLREE (La-Nd). The apatite analysed in this study is plotted on this diagram as small white squares and plots exclusively in the HM field.

https://doi.org/10.5194/egusphere-2024-2034
Preprint. Discussion started: 15 July 2024

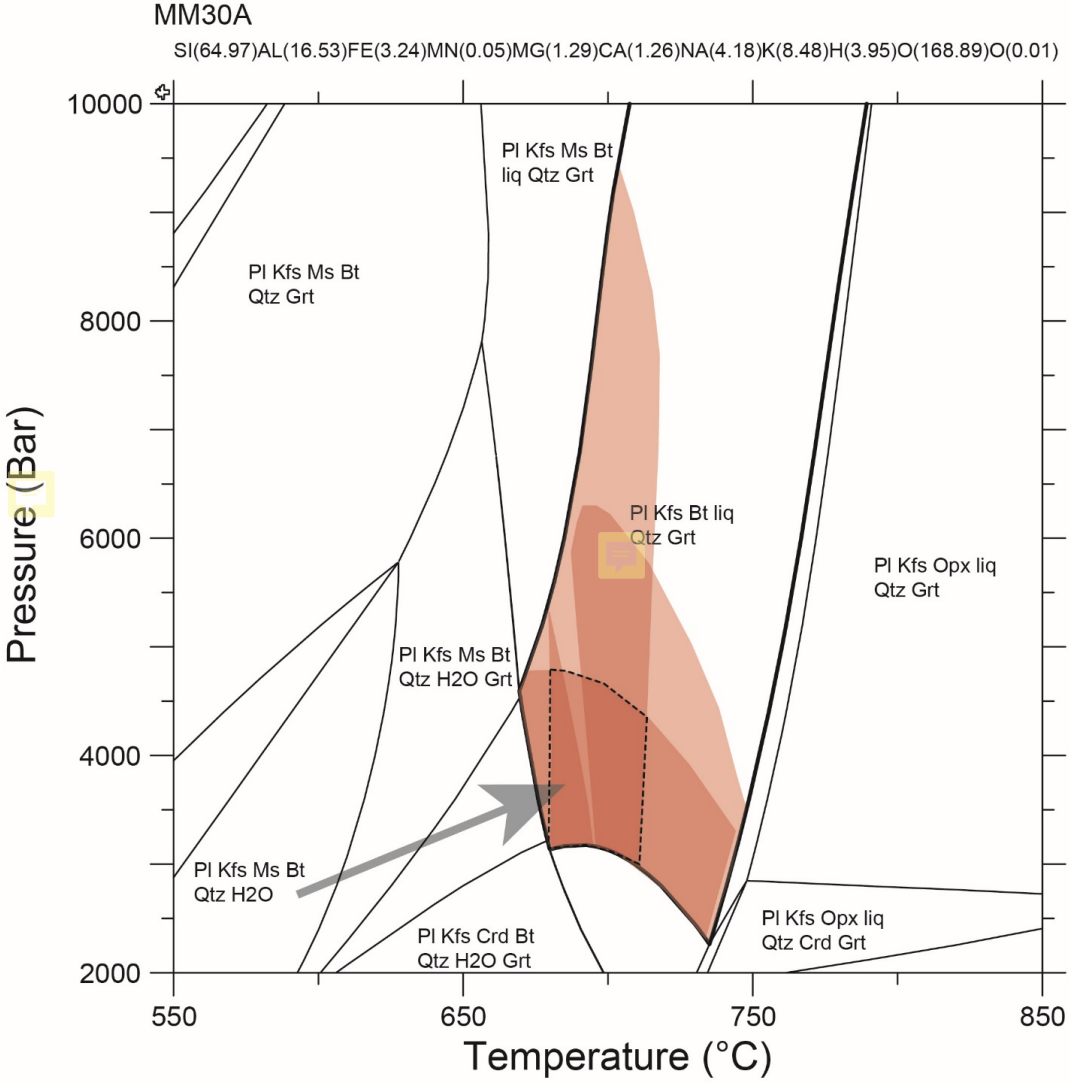

Figure 10. P-T pseudosection for sample MM30A using the bulk composition shown at the top of the diagram (see Table S1). The T-X_{H2O} and T-X_{CaO} diagrams used to investigate this composition are given as Fig. S5 and S6. The shaded red areas indicate regions matching the garnet composition observed in the sample (X_{Alm}: 0.8-0.78; X_{Pyr}: 0.12-0.1; X_{Sps}: 0.1-0.08; X_{Grs}<0.04). The black dashed box is the field of overlap and the grey arrow indicates the direction of increasing garnet mode.

5 Discussion

5.1 Significance of the age data and metamorphic constraints

The garnet Lu-Hf data produces an age of 1834 ± 7 Ma with an MSWD of 1.2 using data from the core and rim of the large garnet as well as all the data from three smaller matrix grains. The low MSWD indicate that this data forms one statistical age population. However, the large garnet cores have an average Lu content of 38 ppm, the large garnet rims have 21 ppm, whereas the small matrix garnets have Lu of 4 ppm. This means that the position of the isochron

https://doi.org/10.5194/egusphere-2024-2034
Preprint. Discussion started: 15 July 2024

is strongly controlled by the core of the large garnet grains, which preserve the highest $^{176}Lu/^{176}Hf$ ratios (red analyses in Fig. 8c). The small matrix garnets give a statistically indistinguishable age of 1857 ± 48 Ma. These matrix garnets are texturally early in comparison with the large leucosome garnet however, the ages are within analytical error, so it is not possible to resolve any age difference using this method. Recently, Smit et al., (2024) show that even at high grade conditions, REE diffuse slowly in natural garnet making Lu-Hf chronology extremely robust. Despite a long and complex history of high-grade metamorphism and magmatism in the region (Väisänen and Hölttä, 1999; Hölttä and Heilimo, 2017; Torvela and Kurhila, 2020), it is likely that the garnet Lu-Hf results reflect growth ages.

The ~~apatite~~ Lu-Hf and U-Pb ages obtained for apatite grains hosted inside large garnets are similar within error, producing ages of 1782 ± 10 Ma and 1778 ± 16 Ma respectively. The Lu-Hf system in apatite is considered to have a higher closure temperature (~670-730 °C; Glorie et al., 2024a) than U-Pb in apatite (350-570 °C; Chew and Spikings, 2021). Thus, a similarity in U-Pb and Lu-Hf ages is indicative of fast cooling at the time of apatite growth. The difference in age between the apatite and the hosting garnet grain (large garnet gave an isochron age of 1829 ± 11 Ma) could indicate that the apatite grains are in contact with the matrix (thus open to grain boundary fluid conduits which may have resulted in resetting at ca. 1780 Ma) or alternatively the sample may have stayed at an elevated temperature (> 700 °C) from ca. 1830 to 1780 Ma.

Mänttäri et al., (2006) obtained U-Pb zircon and monazite ages from the same TGG gneiss unit sampled in this study (sample site 2006 in Fig. 2). Zircon U-Pb data indicate an intrusive age of ca. 1860 Ma for the tonalite with Archean (ca. 2.7 Ga) and Paleoproterozoic (2.0-1.9 Ga) inheritance. Pegmatitic granite dykes present zircon ages of ca. 1830-1790 Ma with interpreted inheritance of Archean (ca. 2.7 Ga) and ca. 1865 Ma. A monazite U-Pb age from a pegmatite of 1823 ± 3 Ma is interpreted as a minimum age for pegmatitic intrusion (Mänttäri et al., 2006).

The P-T diagram for sample MM30A indicates peak P-T conditions ~~of~~ 3-5 kbar and ~~around~~ 700 °C. This result is consistent with previous studies in the region (Tuisku and Kärki, 2010), which indicate regional conditions of 3.5-4 kbar and 660 to 700 °C. The arrow in Figure 10 indicates a proposed prograde P-T path defined by the increase in garnet mode. The P-T path is also parallel to grossular compositional isopleths, producing flat compositional zonation in X_{Grs} along this path, as well as an increase in X_{Pyr} and decrease in X_{Sps} consistent with the compositional zonation observed in the sample.

Based on the interpretation above that the garnet ages likely represent growth ages, representing a period of prograde evolution that occurred at 1834 ± 7 Ma. The large apatite grains that occur as inclusions at the rim of the large garnet preserve Lu-Hf and U-Pb ages of 1782 ± 10 Ma and 1778 ± 16 Ma. As discussed above, this presents two options for the metamorphic evolution of the sample. Either the sample cooled from peak conditions at ca. 1830 Ma and was then reheated to nearly identical conditions at ca. 1780 Ma or high temperature conditions persisted from 1830 to 1780 Ma at which point, rapid cooling from 700 to 400-500 °C (closure T of U-Pb in apatite) occurred. The latter result would be consistent with a regional high temperature, low pressure event. Potentially these conditions persisted for ca. 50 Ma until tectonic uplift, or potentially orogenic collapse, resulted in rapid cooling from 700 to around 400 °C, at ca. 1780 Ma.

5.2 The role of Olkiluoto region in the tectonic setting of S Finland

The P-T-t conditions of Olkiluoto are summarized in Figure 11, and a comparison to surrounding tectonic belts is shown. The Tampere Belt experienced greenschist to amphibolite facies conditions with peak metamorphism interpreted to occur at c. 1.88 Ga (Mouri et al., 1999). Lahtinen et al., (2017) also obtained a garnet age from a mica schist of 1.81 Ga, which they suggest indicates that high grade conditions continued until this time. The Pirkanmaa Belt contains upper amphibolite to granulite facies rocks, that experienced peak metamorphic conditions of 4-5 kbar and 750-700 °C at ca. 1.88 Ga (Mouri et al., 1999). There is also evidence of younger monazite (ca. 1850, Hölttä et al., 2020) and a range of garnet Sm-Nd ages from 1890 to 1840 Ma (Lahtinen et al., 2017; Mouri et al., 1999). The Häme Belt is characterized by greenschist to upper amphibolite facies with peak conditions of 3-4 kbar and 530-580

https://doi.org/10.5194/egusphere-2024-2034
Preprint. Discussion started: 15 July 2024

°C (Hölttä and Heilimo, 2017) in the western Häme Belt, while the eastern Häme Belt preserves upper amphibolite facies conditions. The age of peak metamorphism is poorly defined but is generally interpreted to have occurred at 1.83-1.80 Ga (Hölttä et al., 2020). Saalmann et al., (2009) indicate that the Häme Belt experienced an earlier compressional event at ca. 1.88-1.86 Ga. The southernmost Uusimaa Belt is proposed to have experienced crustal extension at 1.86-1.84 Ga, followed by a transpressional event producing granulite facies peak conditions of 4-5 kbar and 750-800 °C at 1.83-1.80 Ga (Mouri et al., 2005; Skyttä and Mänttäri, 2008).

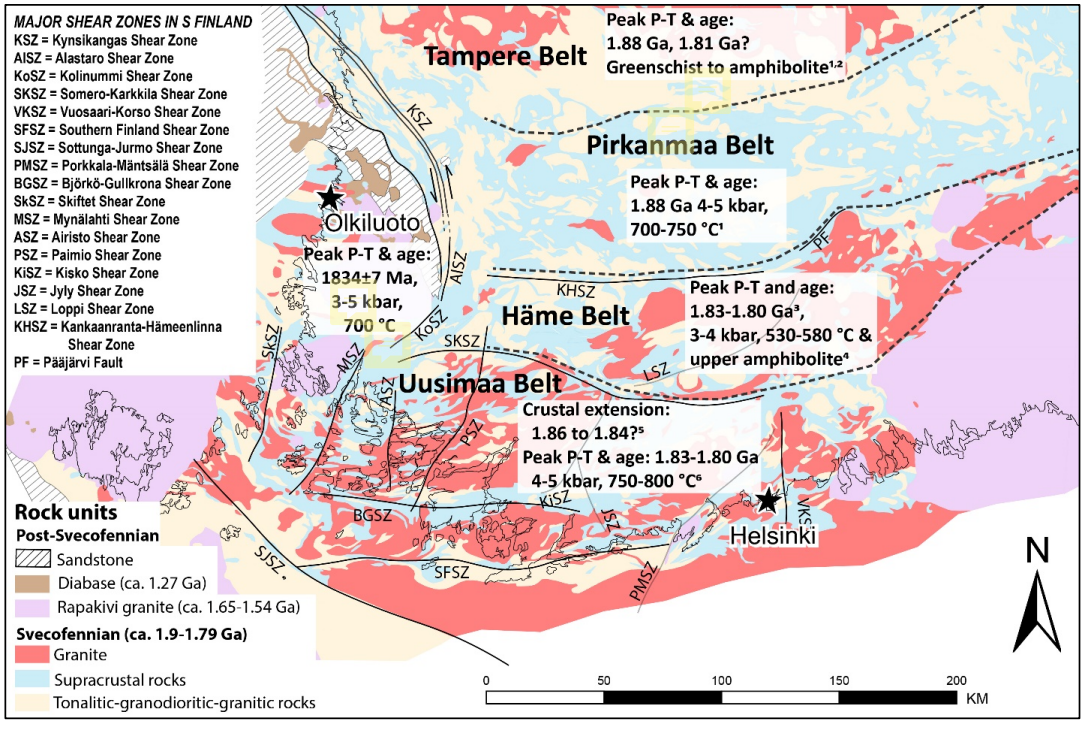

Figure 11. The geological map of S Finland with the different tectonic and metamorphic belts and significant shear zones. The metamorphic ages are compiled from U-Pb monazite Ma ages published in Hölttä et al., (2020). Bedrock map scale 1:200 000, from Geological Survey of Finland (Geological Survey of Finland, 2022). Shear zones adapted from Heeremans et al., 1996; Väisänen and Skyttä, (2007); Torvela et al., (2008); Väisänen et al., (2014); Reimers et al., (2018); Pitkälä, (2019); Torvela and Kurhila, (2022); Lahtinen et al., (2023). The peak P-T conditions and metamorphic ages are derived from the following references: 1) Mouri et al., (1999), 2) Lahtinen et al., (2017), 3) Hölttä et al., (2020), 4) Hölttä and Heilimo, (2017), 5) Skyttä and Mänttäri, (2008) and 6) Mouri et al., (2005).

The Olkiluoto region and Häme Belt have similar crystallisation ages as well as metamorphic and tectonic history during the ca. 1.88-1.79 Ga Svecofennian orogeny. Previous metamorphic studies have shown that the Häme Belt, situated ca. 75 km SE from Olkiluoto (Fig. 11), contains supracrustal rocks that have been interpreted to have two metamorphic peaks: first in amphibolite facies conditions at ca. 1.88-1.86 Ga (Nironen, 1999; Väisänen et al., 2002; Kähkönen, 2005; Kara et al., 2021) and the latter during a high-T event that peaked at ca. 1.83-1.81 Ga (Väisänen et al., 2002). Kurhila et al. (2011) defined that S Finland was subjected to a ~~long-hot~~ anatexis with the emplacement of late-orogenic leucogranites, while Torvela and Kurhila (2022) concluded that the late-orogenic event was coupled to migmatitization and formation of major shear zones in a transpressional tectonic regime (Fig. 11). Our novel garnet and apatite Lu-Hf age data, coupled with ~~metamorphic~~ modelling and previous studies on structural setting (Engström et al., 2022) supports the same evolution. The age indicated by the Lu-Hf geochronology (1834 ± 7 Ma) of the garnets

https://doi.org/10.5194/egusphere-2024-2034
Preprint. Discussion started: 15 July 2024

mainly shows the latter distinct metamorphic peak for the Olkiluoto site, and the structural and metamorphic evolution is in accordance with other studies from the Häme Belt (Kähkönen, 2005; Hölttä and Heilimo, 2017; Kara et al., 2021; Lahtinen et al., 2023).

The study by Saalmann et al., (2009) defined that the latter observed metamorphic peak in Häme Belt was followed by a hydrothermal event with formation of shear zones and mineralization. Even though no mineralization indicative of a hydrothermal event is observed in the Olkiluoto site, a similar hydrothermal and shearing-induced event ~~can be observed with~~ the formation of a certain type of diatexitic migmatite with roundish quartz-feldspar megacrysts (Engström et al., 2022), which are interpreted to be related to the prolonged cooling after the peak P-T conditions of 3-5 kbar and around 700 °C (this study). Temporally simultaneously, the Uusimaa Belt (Fig. 11) mainly underwent granulite facies metamorphism at ca. 1.84-1.81 Ga (Väisänen et al., 2002; Mouri et al., 2005; Skyttä and Mänttäri, 2008) ~~inferring~~ slightly deeper crustal depth ~~for the metamorphism~~ than the Häme Belt (this study 3-5 kbar and around 700 °C), although probably representing a similar geothermal gradient. The interpretation further south in Uusimaa Belt, where shear zones and the anatectic melt are strongly coupled to each other (Torvela and Kurhila, 2020; Lahtinen et al., 2023), indicates that the whole S Finland domain was subjected to a long hot orogenic evolution with several crustal-scale melt pulses.

5.3 Implications for S Finland tectonic framework

The tectonic framework for S Finland possibly represents the distal regions in a back-arc basin complex that formed above the retreated subduction zone in the west, and slab rollback caused (oblique) extension in the upper plate and asthenospheric upwelling in backarc regions, following the proposed models (Collins, 2002; Hermansson et al., 2008; Saalmann et al., 2009; Kara et al., 2021). This caused high heat flow and decompression melting and mafic underplating of the thinned continental crust, giving rise to melt production and intense magmatic activity as well as granulite facies metamorphism in its deeper parts (Väisänen and Hölttä, 1999). This infers different crustal depths for the Häme Belt and Uusimaa Belt (Saalmann et al., 2009; Torvela and Kurhila, 2020). The presence of several shear zones in S Finland is indicative of a transpressive tectonic regime that could be explained by strain partitioning in the oblique tectonic regime where contractional segments were coupled to folding and thrusting, which is observed especially in the Häme Belt (Nironen, 1999; Saalmann et al., 2009; Pitkälä, 2019; Kara et al., 2021). Additionally, in the Uusimaa Belt, where the tectonic regime exhibits more transtensional shear zones (Väisänen and Skyttä, 2007; Torvela and Kurhila, 2022). The mosaic structure with shear zones and different crustal blocks characteristic for S Finland shows that detailed comprehensive studies coupling to both, structural geology and metamorphic studies is essential when determining the character and tectonic evolution of the crystalline bedrock in a high-grade environment that is prevailing in this tectonic domain. The impact of these crustal scale shear zones in the tectonic framework of S Finland is evident, but the kinematic constraints and age relationships are still poorly understood. However, most of these shear zones show ductile deformation signatures inferring deeper and hotter origin, indicating formation before the ductile-brittle transition interpreted at ca. 1.78 Ga (Nordbäck et al., 2024).

5.4 Connection to Ljusdal lithotectonic unit

This study is an additional piece ~~in~~ the puzzle to better understand the missing link between central E Sweden and SW Finland crustal units. Only a limited number of studies are available, and clearly more studies are needed especially in the Bothnian Basin separating Sweden and Finland to unravel if e.g., a failed rifting event is the cause of the separation and why sedimentary units ~~are interpreted~~ offshore (Buntin et al., 2019; Korja and Heikkinen, 2005; Fig 1). Structural studies from SW Finland by Nordbäck et al. (2024) emphasize that large N-S structures are related to this rifting and to development of Mesoproterozoic sedimentary basin at the centre of Fennoscandian shield, located beneath the Bothnian Sea (e.g. Kohonen and Rämö, 2005). Thus, it is reasonable to assume that prior to this rifting event central E Sweden and SW Finland ~~was~~ connected as proposed by Engström et al., (2022) and by Luth et al., (2024) in the lithotectonic map of Fennoscandia. Further evidence is supported by the presence of similar mineralogy

https://doi.org/10.5194/egusphere-2024-2034
Preprint. Discussion started: 15 July 2024

cordierite–sillimanite–garnet mineral assemblage, in both Ljusdal and Olkiluoto (Högdahl and Bergman, 2020; Engström et al., 2022). The prolonged ductile deformation with several crustal-scale melt pulses indicates that the Olkiluoto site is similar to the Ljusdal lithotectonic unit in central E Sweden (Fig. 1) (Engström et al., 2022; Högdahl et al., 2012). Earlier studies by Engström et al., (2022) and Saukko et al., (2020) defined that the area was subjected to a high-grade migmatitic ~~environment~~ during an approximate time span of 90 Ma between 1.87–1.78 Ga, with two main migmatite-producing events. Hence it is plausible, that the Häme Belt, including the Olkiluoto site, is connected to the Ljusdal lithotectonic unit. The major crustal-scale Kynsikangas shear zone located 40 km NE of Olkiluoto possible possibly marks the tectonic boundary between the lithotectonic units (Fig. 11) (Engström et al., 2022). The Saimaa orocline is deduced as a big suture zone between WFS and SFS in studies in E Finland (Lahtinen et al., 2022) and a likely continuation of that is the Kynsikangas shear zone with a possible continuation to the Hassela shear zone in central E Sweden (Reimers et al., 2018; Högdahl and Bergman, 2020; Lahtinen et al., 2023).

6 Conclusions

The previously published structural data (Engström et al., 2022) together with the metamorphic data presented in this paper, suggest that the Häme Belt including the Olkiluoto area and the Ljusdal lithotectonic unit, share a similar deformation history and metamorphic P-T-t conditions (Högdahl et al., 2008; Högdahl and Bergman, 2020; Saukko et al., 2020; Hölttä and Heilimo, 2017; Lahtinen et al., 2023; Luth et al., 2024). Both areas show a younger ca. 1.83 Ga amphibolite-facies metamorphic peak and possibly an older ca. 1.86 Ga metamorphic event.

The main outcome from this study are as follows:

- The garnets in the TGG type rock at the Olkiluoto site were studied and *in situ* Lu-Hf geochronology defined a metamorphic peak at 1834 ± 7 Ma.
- The P-T modelling at the site indicates peak P-T conditions of 3-5 kbar and around 700 °C.
- The metamorphic evolution in S Finland is poorly constrained due to complex structural geological evolution. This study provides valuable input to better constrain the difference between the Häme Belt and Uusimaa Belt.
- The Olkiluoto site is well located between S Finland and Central E Sweden and thus represents a key location to define a missing link between the Swedish and Finnish lithotectonic units. This study presents new results coupling these areas together.

Credit authorship contribution statement:

Jon Engström: Conceptualization, Methodology, Interpretation, Visualization, Writing - original draft **Kathryn Cutts**: Conceptualization, Methodology, Interpretation, Visualization, Writing - review & editing. **Stijn Glorie**: *In situ* Lu-Hf geochronology, Validation, Writing - review. **Esa Heilimo:** Whole-rock geochemistry, Writing - review & editing. **Ester M. Jolis:** Micro-XRF analysis, Writing - review. **Radoslaw M. Michallik:** EPMA analysis, Writing - review.

Competing interests

The contact author has declared that none of the authors has any competing interests.

Acknowledgements

We are grateful to Posiva Oy for the support during the field work, and access to the data. Micro-XRF was supported by the Academy of Finland via RAMI infrastructure project (#337560).

https://doi.org/10.5194/egusphere-2024-2034
Preprint. Discussion started: 15 July 2024

Supplementary data

1. Supplementary Figures
2. Supplementary Table

https://doi.org/10.5194/egusphere-2024-2034
Preprint. Discussion started: 15 July 2024

References

Aaltonen, I., Engström, J., Front, K., Gehör, S., Kosunen, P., Kärki, A., Mattila, J., Paananen, M., Paulamäki, S., 2016. Geology of Olkiluoto (Posiva Report). Posiva Oy, Eurajoki.

Bergman, S., Högdahl, K., Nironen, M., Ogenhall, E., Sjöström, H., Lundqvist, L., Lahtinen, R., 2008. Timing of Palaeoproterozoic intra-orogenic sedimentation in the central Fennoscandian Shield; evidence from detrital zircon in metasandstone. Precambrian Res. 161, 231–249. https://doi.org/10.1016/j.precamres.2007.08.007

Brown, D.A., Simpson, A., Hand, M., Morrisey, L.J., Gilbert, S., Tamblyn, R., Glorie, S., 2022. Laser-ablation Lu-Hf dating reveals Laurentian garnet in subducted rocks from southern Australia. Geology 50, 837–842. https://doi.org/10.1130/G49784.1

Buntin, S., Malehmir, A., Koyi, H., Högdahl, K., Malinowski, M., Larsson, S.Å., Thybo, H., Juhlin, C., Korja, A., Górszczyk, A., 2019. Emplacement and 3D geometry of crustal-scale saucer-shaped intrusions in the Fennoscandian Shield. Nat. Sci. Rep. 9. https://doi.org/10.1038/s41598-019-46837-x

Capitani, C. de, Petrakakis, K., 2010. The computation of equilibrium assemblage diagrams with Theriak/Domino software. Am. Mineral. 95, 1006–1016. https://doi.org/10.2138/am.2010.3354

Chew, D.M., Petrus, J.A., Kamber, B.S., 2014. U–Pb LA–ICPMS dating using accessory mineral standards with variable common Pb. Chem. Geol. 363, 185.

Chew, D.M., Spikings, R.A., 2021. Apatite U-Pb Thermochronology: A Review. Minerals 11, 1095. https://doi.org/10.3390/min11101095

Chopin, F., Korja, A., Nikkilä, K., Hölttä, P., Korja, T., Zaher, M.A., Kurhila, M., Eklund, O., Rämö, O.T., 2020. The Vaasa Migmatitic Complex (Svecofennian Orogen, Finland): Buildup of a LP-HT Dome During Nuna Assembly. Tectonics 39, e2019TC005583. https://doi.org/10.1029/2019TC005583

Collins, W.J., 2002. Hot orogens, tectonic switching, and creation of continental crust. Geology 30, 535–538. https://doi.org/10.1130/0091-7613(2002)030<0535:HOTSAC>2.0.CO;2

Engström, J., Kärki, A., Paulamäki, S., Mänttäri, I., 2022. Palaeoproterozoic structural evolution of polyphase migmatites in Olkiluoto, SW Finland. Bull. Geol. Soc. Finl. 94 (1–2), 119–144. https://doi.org/10.17741/bgsf/94.2.002

Geological Survey of Finland, 2022. Geological bedrock map of Finland.

Gillespie, J., Glorie, S., Khudoley, A., Collins, A., 2018. Detrital apatite U-Pb and trace element analysis as a provenance tool: insights from the Yenisey Ridge (Siberia). http://dx.doi.org/10.1016/j.lithos.2018.05.026. https://doi.org/10.1016/j.lithos.2018.05.026

Glorie, S., Gillespie, J., Simpson, A., Gilbert, S., Khudoley, A., Priyatkina, N., Hand, M., Kirkland, C.L., 2022. Detrital apatite Lu–Hf and U–Pb geochronology applied to the southwestern Siberian margin. Terra Nova 34, 201–209. https://doi.org/10.1111/ter.12580

Glorie, S., Hand, M., Mulder, J., Simpson, A., Emo, R.B., Kamber, B., Fernie, N., Nixon, A., Gilbert, S., 2024a. Robust laser ablation Lu–Hf dating of apatite: an empirical evaluation. Geol. Soc. Lond. Spec. Publ. 537, 165–184. https://doi.org/10.1144/SP537-2022-205

Glorie, S., Simpson, A., Gilbert, S.E., Hand, M., Müller, A.B., 2024b. Testing the reproducibility of in situ Lu-Hf dating using Lu-rich garnet from the Tørdal pegmatites, southern Norway. Chem. Geol. 653, 122038. https://doi.org/10.1016/j.chemgeo.2024.122038

Glorie, S.M., Jepson, G., Konopelko, D., Mirkamalov, R., Meeuws, F., Gilbert, S., Gillespie, J., Collins, A., Xiao, W., Dewaele, S., De Grave, J., 2019. Thermochronological and geochemical footprints of post-orogenic fluid alteration recorded in apatite: implications for mineralisation in the Uzbek Tian Shan. http://dx.doi.org/10.1016/j.gr.2019.01.011. https://doi.org/10.1016/j.gr.2019.01.011

Heeremans, M., Stel, H., Van Der Beek, P., Lankreijer, A., 1996. Tectono-magmatic control on vertical dip slip basement faulting: An example from the Fennoscandian Shield. Terra Nova 8, 129–140. https://doi.org/10.1111/j.1365-3121.1996.tb00737.x

Heilimo, E., Mikkola, P., Ahven, M., Huhma, H., Lahaye, Y., Virtanen, V.J., 2023. Evidence of crustal growth during the Svecofennian orogeny: New isotopic data from the central parts of the Paleoproterozoic Central Finland Granitoid Complex. Precambrian Res. 395, 107125. https://doi.org/10.1016/j.precamres.2023.107125

Hermansson, T., Stephens, M.B., Corfu, F., Page, L.M., Andersson, J., 2008. Migratory tectonic switching, western Svecofennian orogen, central Sweden: Constraints from U/Pb zircon and titanite geochronology. Precambrian Res. 161, 250–278. https://doi.org/10.1016/j.precamres.2007.08.008

Hietanen, A., 1975. Generation of potassium-poor magmas in the northern Sierra Nevada and the Svecofennian in Finland. J. Res. US Geol. Surv. 1975, 631–645.

https://doi.org/10.5194/egusphere-2024-2034
Preprint. Discussion started: 15 July 2024

Högdahl, K., Bergman, S., 2020. Chapter 5 Paleoproterozoic (1.9–1.8 Ga), syn-orogenic magmatism and sedimentation in the Ljusdal lithotectonic unit, Svecokarelian orogen. Geol. Soc. Lond. Mem. 50, 131–153. https://doi.org/10.1144/M50-2016-30

Högdahl, K., Majka, J., Sjöström, H., Nilsson, K.P., Claesson, S., Konečný, P., 2012. Reactive monazite and robust zircon growth in diatexites and leucogranites from a hot, slowly cooled orogen: implications for the Palaeoproterozoic tectonic evolution of the central Fennoscandian Shield, Sweden. Contrib. Mineral. Petrol. 163, 167–188. https://doi.org/10.1007/s00410-011-0664-x

Högdahl, K., Sjöström, H., Andersson, U.B., Ahl, M., 2008. Continental margin magmatism and migmatisation in the west-central Fennoscandian Shield. Lithos 102, 435–459. https://doi.org/10.1016/j.lithos.2007.07.019

Holland, T., Powell, R., 2003. Activity–composition relations for phases in petrological calculations: an asymmetric multicomponent formulation. Contrib. Mineral. Petrol. 145, 492–501. https://doi.org/10.1007/s00410-003-0464-z

Holland, T.J.B., Powell, R., 2011. An improved and extended internally consistent thermodynamic dataset for phases of petrological interest, involving a new equation of state for solids. J. Metamorph. Geol. 29, 333–383. https://doi.org/10.1111/j.1525-1314.2010.00923.x

Hölttä, P., Heilimo, E., 2017. Metamorphic Map of Finland. Spec. Pap. - Geol. Surv. Finl. 60, 75–126.

Hölttä, P., Huhma, H., Lahaye, Y., Mänttäri, I., Lukkari, S., O'Brien, H., 2020. Paleoproterozoic metamorphism in the northern Fennoscandian Shield: age constraints revealed by monazite. Int. Geol. Rev. 62, 360–387. https://doi.org/10.1080/00206814.2019.1611488

Irvine, T.N., Baragar, W.R.A., 1971. A Guide to the Chemical Classification of the Common Volcanic Rocks. Can. J. Earth Sci. 8, 523–548. https://doi.org/10.1139/e71-055

Jørgensen, T.R.C., Tinkham, D.K., Lesher, C.M., 2019. Low-P and high-T metamorphism of basalts: Insights from the Sudbury impact melt sheet aureole and thermodynamic modelling. J. Metamorph. Geol. 37, 271–313. https://doi.org/10.1111/jmg.12460

Kähkönen, Y., 2005. Chapter 8 Svecofennian supracrustal rocks, in: Lehtinen, M., Nurmi, P.A., Rämö, O.T. (Eds.), Developments in Precambrian Geology, Precambrian Geology of Finland Key to the Evolution of the Fennoscandian Shield. Elsevier, pp. 343–405. https://doi.org/10.1016/S0166-2635(05)80009-X

Kara, J., Leskelä, T., Väisänen, M., Skyttä, P., Lahaye, Y., Tiainen, M., Leväniemi, H., 2021. Early Svecofennian rift-related magmatism: Geochemistry, U-Pb-Hf zircon isotope data and tectonic setting of the Au-hosting Uunimäki gabbro, SW Finland. Precambrian Res. 364, 106364. https://doi.org/10.1016/j.precamres.2021.106364

Kärki, A., 2015. Migmatites and Migmatite-Like Rocks of Olkiluoto (Working Report No. 2015– 03), Posiva Working Report. Posiva Oy, Eurajoki.

Kohonen, J., Lahtinen, R., Luukas, J., Nironen, M., 2021. Classification of regional-scale tectonic map units in Finland. Geol. Surv. Finl. Bull. 33–80. https://doi.org/10.30440/bt412.2

Kohonen, J., Rämö, O.T., 2005. Chapter 13 Sedimentary rocks, diabases, and late cratonic evolution, in: Lehtinen, M., Nurmi, P.A., Rämö, O.T. (Eds.), Developments in Precambrian Geology, Precambrian Geology of Finland Key to the Evolution of the Fennoscandian Shield. Elsevier, pp. 563–603. https://doi.org/10.1016/S0166-2635(05)80014-3

Koistinen, T., Bogatchev, V., Stephens, M.B., Nordgulen, O., Wennerström, M., Korhonen, J., 2001. Geological map of the Fennoscandian Shield scale 1:2 000 000.

Korja, A., Heikkinen, P., 2005. The accretionary Svecofennian orogen—insight from the BABEL profiles. Precambrian Res. 136, 241–268. https://doi.org/10.1016/j.precamres.2004.10.007

Korsman, K., Koistinen, T., Kohonen, J., Wennerström, M., Ekdahl, E., Honkamo, M., Idman, H., 1997. Suomen kallioperäkartta = Berggrundskarta över Finland = Bedrock map of Finland.

Korsman, K., Korja, T., Pajunen, M., Virransalo, P., GGT/SVEKA Working Group, 1999. The GGT/SVEKA Transect: Structure and Evolution of the Continental Crust in the Paleoproterozoic Svecofennian Orogen in Finland. Int. Geol. Rev. 41, 287–333. https://doi.org/10.1080/00206819909465144

Kurhila, M., Mänttäri, I., Vaasjoki, M., Tapani Rämö, O., Nironen, M., 2011. U-Pb geochronological constraints of the late Svecofennian leucogranites of southern Finland. Precambrian Res. 190, 1–24. https://doi.org/10.1016/j.precamres.2011.07.008

Lahtinen, R., Huhma, H., Sipilä, P., Vaarma, M., 2017. Geochemistry, U-Pb geochronology and Sm-Nd data from the Paleoproterozoic Western Finland supersuite – A key component in the coupled Bothnian oroclines. Precambrian Res. 299, 264–281. https://doi.org/10.1016/j.precamres.2017.07.025

Lahtinen, R., Korja, A., Nironen, M., 2005. Palaeoproterozoic tectonic evolution of the Fennoscandian Shield. Precambrian Geol. Finl. -Key Evol. Fennoscandian Shield Dev. Precambrian Geol. 14, 418–532.

https://doi.org/10.5194/egusphere-2024-2034
Preprint. Discussion started: 15 July 2024

Lahtinen, R., Köykkä, J., Salminen, J., Sayab, M., Johnston, S.T., 2023. Paleoproterozoic tectonics of Fennoscandia and the birth of Baltica. Earth-Sci. Rev. 104586. https://doi.org/10.1016/j.earscirev.2023.104586

Lahtinen, R., Salminen, P.E., Sayab, M., Huhma, H., Kurhila, M., Johnston, S.T., 2022. Age and structural constraints on the tectonic evolution of the Paleoproterozoic Saimaa orocline in Fennoscandia. Precambrian Res. 369, 106477. https://doi.org/10.1016/j.precamres.2021.106477

Lanari, P., Vidal, O., De Andrade, V., Dubacq, B., Lewin, E., Grosch, E.G., Schwartz, S., 2014. XMapTools: A MATLAB©-based program for electron microprobe X-ray image processing and geothermobarometry. Comput. Geosci. 62, 227–240. https://doi.org/10.1016/j.cageo.2013.08.010

Lane, K.M., 2011. Metamorphic and geochronological constraints on the evolution of the Kalinjala Shear Zone, Eyre Peninsula (PhD Thesis). University of Adelaide.

Li, Y., Vermeesch, P., 2021. Short communication: Inverse isochron regression for Re–Os, K–Ca and other chronometers. Geochronology 3, 415–420. https://doi.org/10.5194/gchron-3-415-2021

Luth, S., Torgersen, E., Köykkä, J., 2024. Lithotectonic map of Fennoscandia, in: In: Regnéll, C., Zack, T., Holme, K. & Andersson, J. (Eds.) 2024: 36th Nordic Geological Winter Meeting, Göteborg. Presented at the Nordic Gelogical Winter Meeting 2024, Geologiska Föreningen Specialpublikation 5, p. 558.

Mäkitie, H., Sipilä, P., Kujala, H., Lindberg, A., Kotilainen, A., 2012. Formation mechanism of the Vaasa Batholith in the Fennoscandian shield: Petrographic and geochemical constraints. Bull. Geol. Soc. Finl. 84, 141–166. https://doi.org/10.17741/bgsf/84.2.003

Mänttäri, I., Talikka, M., Paulamäki, S., Mattila, J., 2006. U-Pb ages for tonalitic gneiss, pegmatitic granite, and diabase dyke, Olkiluoto study site, Eurajoki, SW Finland (Working Report No. 2006–12), Posiva Working Report. Posiva Oy, Eurajoki.

Mark, C., O'Sullivan, G., Glorie, S., Simpson, A., Andò, S., Barbarano, M., Stutenbecker, L., Daly, J.S., Gilbert, S., 2023. Detrital Garnet Geochronology by In Situ U-Pb and Lu-Hf Analysis: A Case Study From the European Alps. J. Geophys. Res. Earth Surf. 128, e2023JF007244. https://doi.org/10.1029/2023JF007244

McDonough, W.F., Sun, S. -s., 1995. The composition of the Earth. Chem. Geol., Chemical Evolution of the Mantle 120, 223–253. https://doi.org/10.1016/0009-2541(94)00140-4

Middlemost, E.A.K., 1994. Naming materials in the magma/igneous rock system. Earth-Sci. Rev. 37, 215–224. https://doi.org/10.1016/0012-8252(94)90029-9

Mouri, H., Korsmän, K., Huhma, H., 1999. Tectono-metamorphic evolution and timing of the melting processes in the Svecofennian Tonalite-Trondhjemite Migmatite Belt: An example from Luopioinen, Tampere area, southern Finland. Bull. Geol. Soc. Finl. 71 (1). https://doi.org/10.17741/bgsf/71.1.003

Mouri, H., Väisänen, M., Huhma, H., Korsman, K., 2005. Sm-Nd garnet and U-Pb monazite dating of high-grade metamorphism and crustal melting in the West Uusimaa area, southern Finland. GFF 127, 123–128. https://doi.org/10.1080/11035890501272123

Nebel, O., Morel, M., Vroon, P., 2009. Isotope Dilution Determinations of Lu, Hf, Zr, Ta and W, and Hf Isotope Compositions of NIST SRM 610 and 612 Glass Wafers. Geostand Geoanal Res 33, 487–499.

Nironen, M., 2017. Bedrock of Finland at the scale 1:1 000 000 – Major stratigraphic units, metamorphism and tectonic evolution, Geological Survey of Finland, Special Paper 60.

Nironen, M., 2005. Chapter 10 Proterozoic orogenic granitoid rocks, in: Lehtinen, M., Nurmi, P.A., Rämö, O.T. (Eds.), Developments in Precambrian Geology, Precambrian Geology of Finland Key to the Evolution of the Fennoscandian Shield. Elsevier, pp. 443–479. https://doi.org/10.1016/S0166-2635(05)80011-8

Nironen, M., 1999. Structural and magmatic evolution in the Loimaa area, southwestern Finland. Bull. Geol. Soc. Finl. Volume 71 (1–2). https://doi.org/10.17741/bgsf/71.1.004

Nironen, M., 1997. The Svecofennian Orogen: A tectonic model. Precambrian Res. 86, 21–44. https://doi.org/10.1016/S0301-9268(97)00039-9

Nordbäck, N., Skyttä, P., Engström, J., Ovaskainen, N., Mattila, J., Aaltonen, I., 2024. Mesoproterozoic Strike-Slip Faulting within the Åland Rapakivi Batholith, Southwestern Finland. τεκτονικα 2, 1–26. https://doi.org/10.55575/tektonika2024.2.1.51

Norris, A., Danyushevsky, L., 2018. Towards estimating the complete uncertainty budget of quantified results measured by LA-ICP-MS. Presented at the Goldschmidt, Boston, USA.

O'Sullivan, G., Chew, D., Kenny, G., Henrichs, I., Mulligan, D., 2020. The trace element composition of apatite and its application to detrital provenance studies. Earth-Sci. Rev. 201, 103044. https://doi.org/10.1016/j.earscirev.2019.103044

Pitkälä, I., 2019. Shear zones and structural analysis of the Loimaa area, SW Finland (M.Sc. Thesis). University of Turku.

https://doi.org/10.5194/egusphere-2024-2034
Preprint. Discussion started: 15 July 2024

Pouchou, J.L., Pichoir, F., 1986. Basic expression of "PAP" computation for quantitative EPMA., in: In: Brown, J.D. & Packwood, R.H. (Eds.) 11 Th International Congress on X - Ray Optics and Microanalysis (ICXOM). pp. 249–253.

Reimers, S., Engström, J., Riller, U., 2018. The Kynsikangas shear zone, Southwest Finland: Importance for understanding deformation kinematics and rheology of lower crustal shear zones, in: Lithosphere 2018 - Tenth Symposium on the Structure, Composition and Evolution of the Lithosphere in Fennoscandia. Programme and Extended Abstracts. INSTITUTE OF SEISMOLOGY UNIVERSITY OF HELSINKI REPORT S-67.

Saalmann, K., Mänttäri, I., Ruffet, G., Whitehouse, M.J., 2009. Age and tectonic framework of structurally controlled Palaeoproterozoic gold mineralization in the Häme belt of southern Finland. Precambrian Res. 174, 53–77. https://doi.org/10.1016/j.precamres.2009.06.005

Saukko, A., Ahläng, C., Nikkilä, K., Soesoo, A., Eklund, O., 2020. Double Power-Law in Leucosome Width Distribution: Implications for Recognizing Melt Movement in Migmatites. Front. Earth Sci. 8. https://doi.org/10.3389/feart.2020.591871

Simpson, A., Gilbert, S., Tamblyn, R., Hand, M., Spandler, C., Gillespie, J., Nixon, A., Glorie, S., 2021. In-situ LuHf geochronology of garnet, apatite and xenotime by LA ICP MS/MS. Chem. Geol. 577, 120299. https://doi.org/10.1016/j.chemgeo.2021.120299

Simpson, A., Glorie, S., Hand, M., Spandler, C., Gilbert, S., 2023. Garnet Lu-Hf speed dating: A novel method to rapidly resolve polymetamorphic histories. Gondwana Res. 121, 215–234. https://doi.org/10.1016/j.gr.2023.04.011

Skyttä, P., Mänttäri, I., 2008. Structural setting of late Svecofennian granites and pegmatites in Uusimaa Belt, SW Finland: Age constraints and implications for crustal evolution. Precambrian Res. 164, 86–109. https://doi.org/10.1016/j.precamres.2008.04.001

Smit, M.A., Vrijmoed, J.C., Scherer, E.E., Mezger, K., Kooijman, E., Schmitt-Kielman, M., Tual, L., Guilmette, C., Ratschbacher, L., 2024. Retentiveness of rare earth elements in garnet with implications for garnet Lu-Hf chronology. J. Metamorph. Geol. n/a, 1–25. https://doi.org/10.1111/jmg.12769

Söderlund, U., Patchett, P.J., Vervoort, J.D., Isachsen, C.E., 2004. The 176Lu decay constant determined by Lu–Hf and U–Pb isotope systematics of Precambrian mafic intrusions. Earth Planet. Sci. Lett. 219, 311–324. https://doi.org/10.1016/S0012-821X(04)00012-3

Spencer, C.J., Kirkland, C.L., Roberts, N.M.W., Evans, N.J., Liebmann, J., 2020. Strategies towards robust interpretations of in situ zircon Lu–Hf isotope analyses. Geosci. Front. 843–853. https://doi.org/10.1016/j.gsf.2019.09.004

Stephens, M.B., 2020. Chapter 1 Introduction to the lithotectonic framework of Sweden and organization of this Memoir. Geol. Soc. Lond. Mem. 50, 1–15. https://doi.org/10.1144/M50-2019-21

Tamblyn, R., Hand, M., Simpson, A., Gilbert, S., Wade, B., Glorie, S., 2022. In situ laser ablation Lu–Hf geochronology of garnet across the Western Gneiss Region: campaign-style dating of metamorphism. J. Geol. Soc. 179, jgs2021-094. https://doi.org/10.1144/jgs2021-094

Thompson, J., Meffre, S., Maas, R., Kamenetsky, V., Kamenetsky, M., Goemann, K., Ehrig, K., Danyushevsky, L., 2016. Matrix effects in Pb/U measurements during LA-ICP-MS analysis of the mineral apatite. J. Anal. At. Spectrom. 31, 1206–1215. https://doi.org/10.1039/C6JA00048G

Thomson, S.N., Gehrels, G.E., Ruiz, J., Buchwaldt, R., 2012. Routine low-damage apatite U-Pb dating using laser ablation–multicollector–ICPMS. Geochem. Geophys. Geosystems 13. https://doi.org/10.1029/2011GC003928

Torvela, T., Kurhila, M., 2022. Timing of syn-orogenic, high-grade transtensional shear zone formation in the West Uusimaa Complex, Finland. Bull. Geol. Soc. Finl. 18. https://doi.org/10.17741/bgsf/94.1.001

Torvela, T., Kurhila, M., 2020. How does orogenic crust deform? Evidence of crustal-scale competent behaviour within the partially molten middle crust during orogenic compression. Precambrian Res. 342, 105670. https://doi.org/10.1016/j.precamres.2020.105670

Torvela, T., Mänttäri, I., Hermansson, T., 2008. Timing of deformation phases within the South Finland shear zone, SW Finland. Precambrian Res. 160, 277–298. https://doi.org/10.1016/j.precamres.2007.08.002

Tuisku, P., Kärki, A., 2010. Metamorphic Petrology of Olkiluoto (Working Report No. 2010–54), Posiva Working Report. Posiva Oy, Eurajoki.

Väisänen, M., Eklund, O., Lahaye, Y., O'Brien, H., Fröjdö, S., Högdahl, K., Lammi, M., 2012. Intra-orogenic Svecofennian magmatism in SW Finland constrained by LA-MC-ICP-MS zircon dating and geochemistry. GFF 134, 99–114. https://doi.org/10.1080/11035897.2012.680606

https://doi.org/10.5194/egusphere-2024-2034
Preprint. Discussion started: 15 July 2024

Väisänen, M., Hölttä, P., 1999. Structural and metamorphic evolution of the Turku migmatite complex, southwestern Finland. Bull. Geol. Soc. Finl. 71, 177–218. https://doi.org/10.17741/bgsf/71.1.009

Väisänen, M., Mänttäri, I., Hölttä, P., 2002. Svecofennian magmatic and metamorphic evolution in southwestern Finland as revealed by U-Pb zircon SIMS geochronology. Precambrian Res. 116, 111–127. https://doi.org/10.1016/S0301-9268(02)00019-0

Väisänen, M., Simelius, C., O'Brien, H., Kyllästinen, M., Mattila, J., 2014. Late Svecofennian mafic magmatism in southern Finland, in: Eight Symposium on Structure, Composition and Evolution of the Lithosphere in Fennoscandia Programme and Extended abstracts. p. 107.

Väisänen, M., Skyttä, P., 2007. Late Svecofennian shear zones in southwestern Finland. GFF 129, 55–64. https://doi.org/10.1080/11035890701291055

Vermeesch, P., 2018. IsoplotR: A free and open toolbox for geochronology. Geosci. Front., SPECIAL ISSUE: Frontiers in geoscience:A tribute to Prof. Xuanxue Mo 9, 1479–1493. https://doi.org/10.1016/j.gsf.2018.04.001

White, R.W., Powell, R., Holland, T.J.B., Johnson, T.E., Green, E.C.R., 2014a. New mineral activity–composition relations for thermodynamic calculations in metapelitic systems. J. Metamorph. Geol. 32, 261–286. https://doi.org/10.1111/jmg.12071

White, R.W., Powell, R., Johnson, T.E., 2014b. The effect of Mn on mineral stability in metapelites revisited: new a–x relations for manganese-bearing minerals. J. Metamorph. Geol. 32, 809–828. https://doi.org/10.1111/jmg.12095

Supplementary Figures

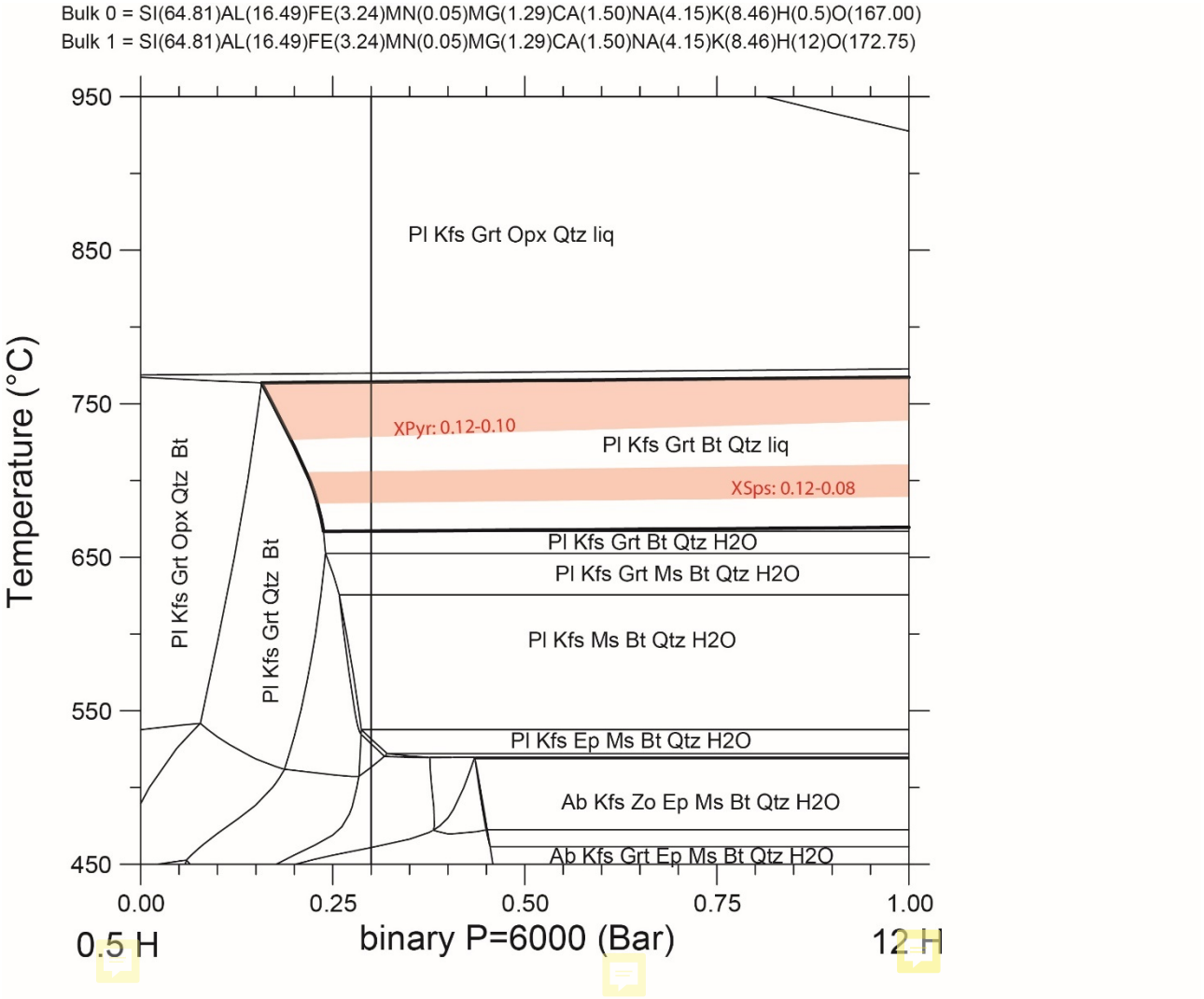

Fig. S1. T-XH2O diagram at 6000 bar for sample MM30A. The interpreted peak assemblage of garnet-plagioclase-biotite-K-feldspar-quartz-melt is highlighted in bold. The red fields indicate the XSps and XPyr compositions that are present in the garnet grains of the sample. The bold line indicates the H2O value used to calculate the TXCaO and P-T diagrams.

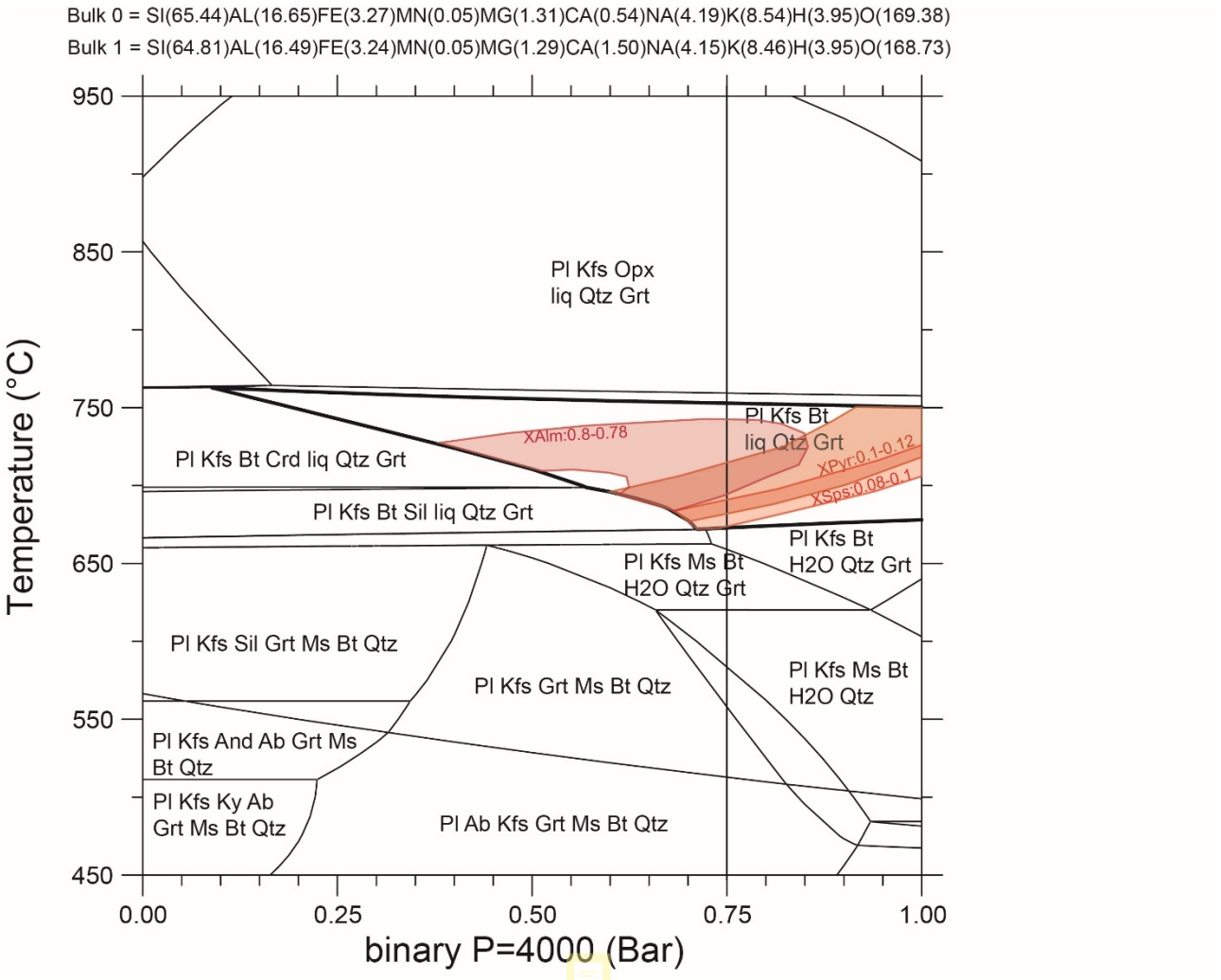

Fig. S2. T-XCaO diagram for sample MM30A at 4000 bar. The interpreted peak assemblage of garnet-plagioclase-biotite-K-feldspar-quartz-melt is highlighted in bold. The red fields indicate the XSps, XPyr and XAlm compositions that are present in the garnet grains of the sample. The bold line indicates the CaO value used to calculate the P-T diagram.

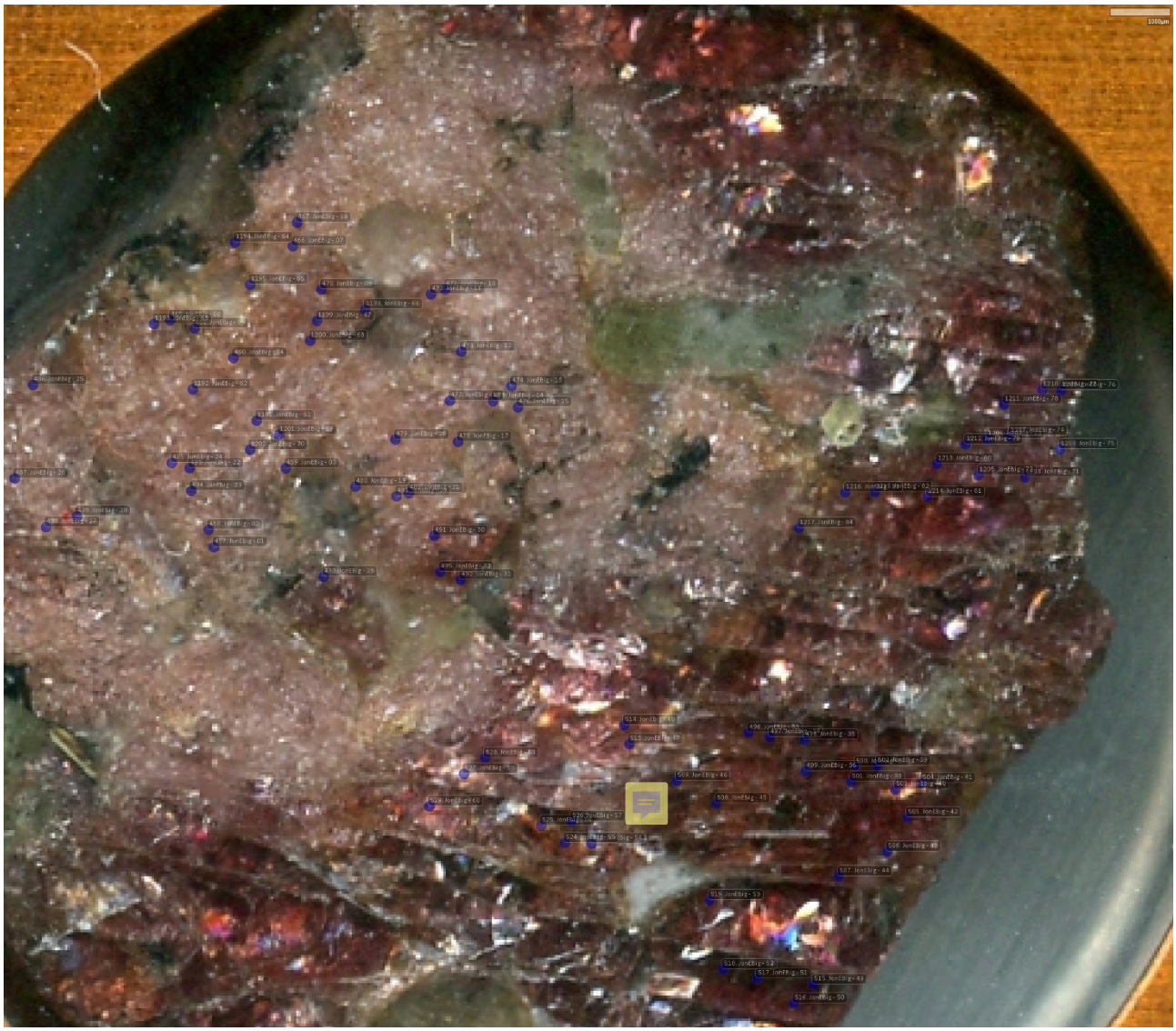

Fig. S3. Lu-Hf spot locations for large garnet.

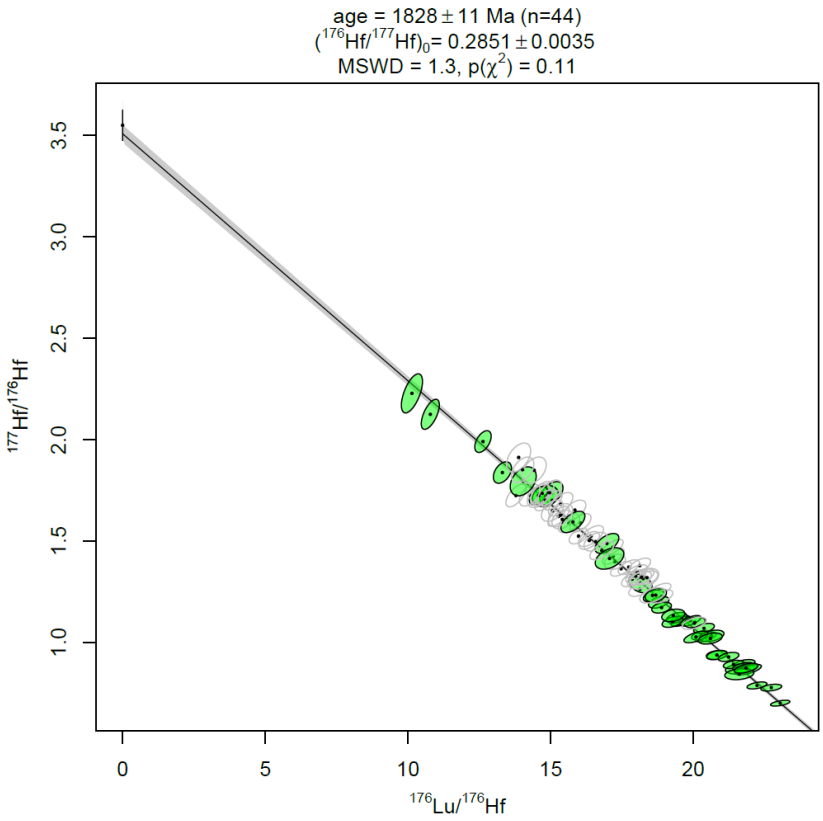

Fig. S4. Calculated Lu-Hf isochron for analyses obtained from the garnet core only.

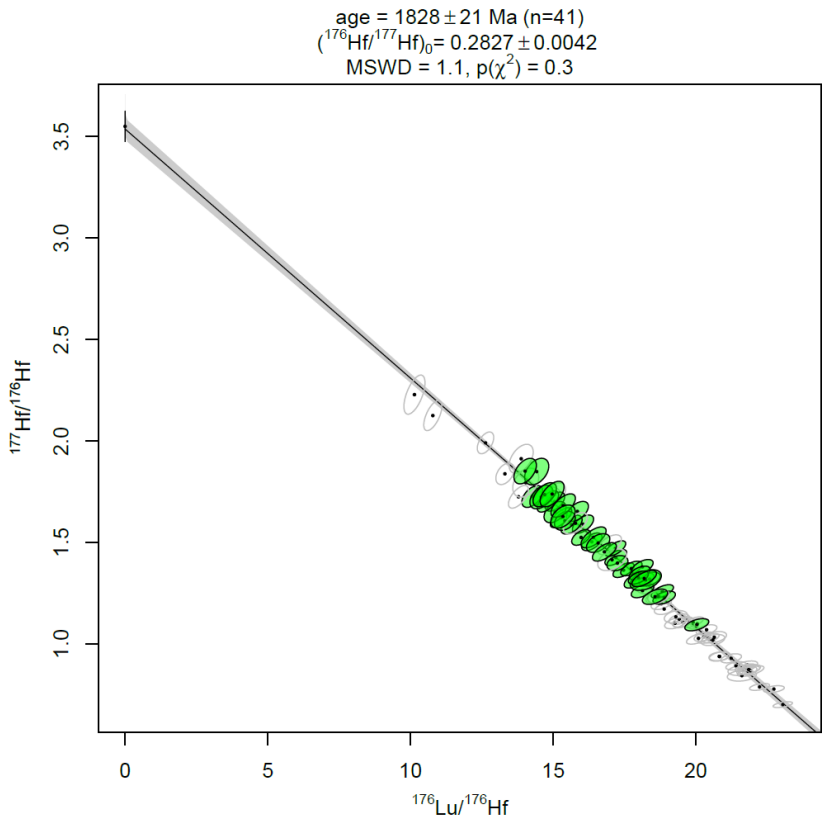

Fig. S5. Calculated Lu-Hf garnet isochron using analyses obtained from the rim only.

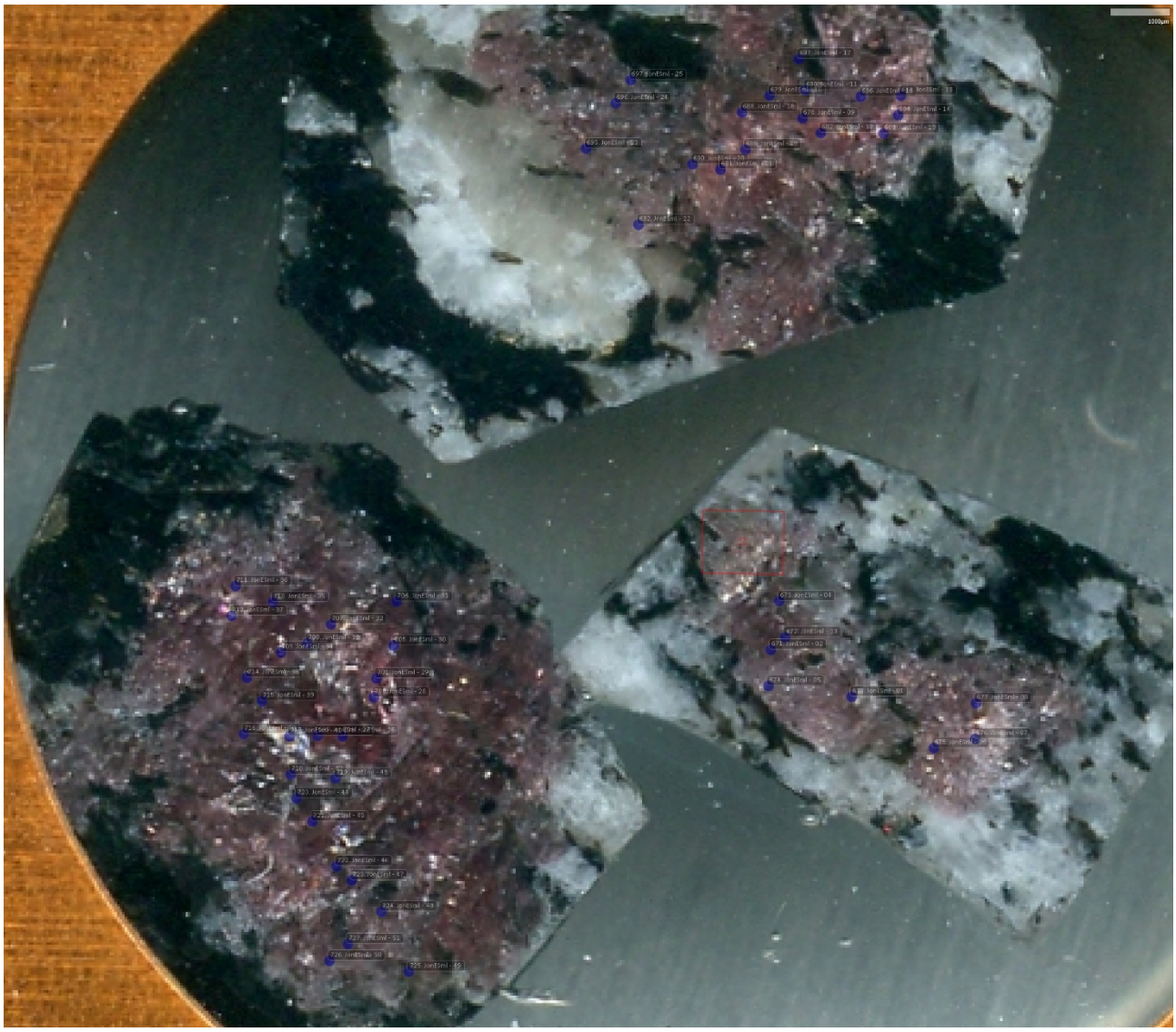

Fig. S6. Lu-Hf spot locations for small garnet.